

Peter van Keken¹

¹Affiliation not available

July 23, 2023

REVIEW

An introductory review of the thermal structure of subduction zones: I. Motivation and selected examples

Peter E. van Keken* and Cian R. Wilson

*Correspondence:

pvankeken@carnegiescience.edu
 Earth and Planets Laboratory,
 Carnegie Institution for Science,
 5241 Broad Branch Road, NW,
 Washington DC 20015, USA.
 Full list of author information is
 available at the end of the article

Abstract

The thermal structure of subduction zones is fundamental to our understanding of physical and chemical processes that occur at active convergent plate margins. These include magma generation and related arc volcanism, shallow and deep seismicity, and metamorphic reactions that can release fluids. Computational models can predict the thermal structure to great numerical precision when models are fully described but this does not guarantee accuracy or applicability. In a pair of companion papers the construction of thermal subduction zone models, their use in subduction zone studies, and their link to geophysical and geochemical observations is explored. In part I the motivation to understand the thermal structure is presented based on experimental and observational studies. This is followed by a description of a selection of thermal models for the Japanese subduction zones.

Keywords

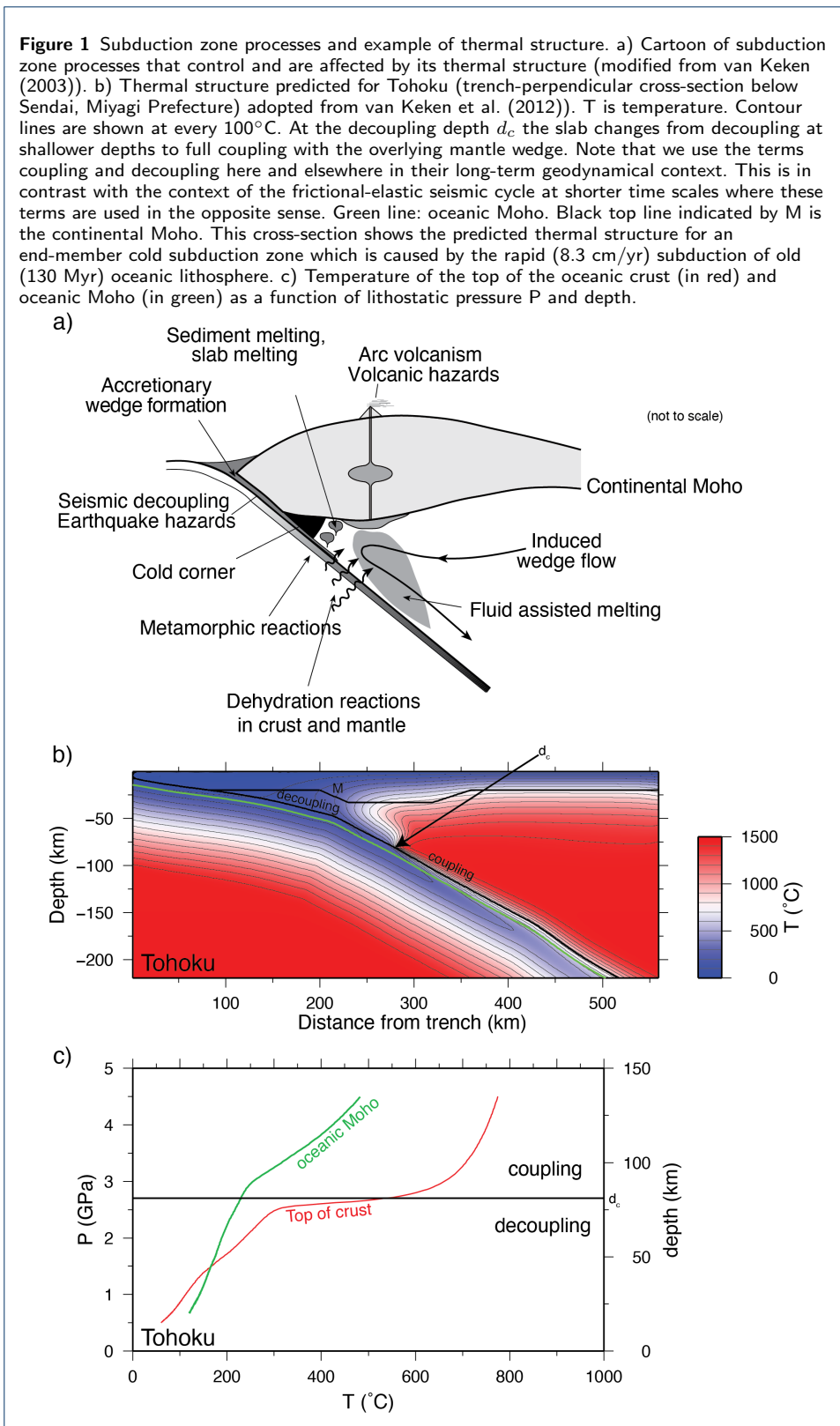
Geodynamics, Plate tectonics, Finite element methods, Subduction zone metamorphism, Arc volcanism

1
2

3 1 Introduction

4 Subduction zones are tectonically active regions on Earth where oceanic plates
 5 descend into the Earth's mantle below a continental or oceanic plate. These are lo-
 6 cations that experience explosive arc volcanism, large underthrusting earthquakes
 7 along the seismogenic zone, and continental crust production. Deeper expression
 8 of subduction are, for example, the metamorphic changes that include dehydra-
 9 tion reactions that lead to melting in the overlying mantle and that can lead to
 10 intermediate-depth and deep seismicity (Figure 1a).

11 The thermal state of subduction zones exerts fundamental controls on volcanic
 12 activity, seismicity, and metamorphic reactions. We will provide an introductory
 13 overview of observational, experimental, and modeling approaches that can be used
 14 to understand the thermal structure of subduction zones and its impact on global
 15 dynamics. We have provided a broad discussion with more detail than is common in
 16 review papers. This is intended to broaden the appeal of this review to an audience
 17 of advanced undergraduate students, graduate students, and any professionals from
 18 outside the field of geodynamics who are interested in an introductory review. We
 19 will focus on modeling details that allow readers to better comprehend how subduc-
 20 tion zone thermal models are formulated, executed, and validated. We will discuss
 21 recent literature in particular to highlight the broad and current interest that the



23 “traditional” reviews see van Keken (2003), Wada and King (2015), and Peacock
24 (2020).

25 1.1 Mechanisms and factors controlling thermal structure

26 The oceanic lithosphere is a rheological boundary layer of the Earth’s solid mantle
27 that is relatively strong compared to the underlying asthenosphere. The lithosphere
28 has petrological distinctions with a ~ 6 km thick crust (Christeson et al., 2019) that
29 overlies a depleted layer of harzburgite from which the melt that formed the crust
30 at mid-oceanic ridges has been extracted. As the oceanic lithosphere spreads from
31 the mid-ocean ridge it ages and cools; at an age of 80–100 Myr the lithosphere
32 reaches a typical thickness of 100 km. Upon subduction, the oceanic lithosphere
33 stops cooling and starts warming due to a combination of processes. Along its
34 entirety, the slab warms due to heat flowing from the warm mantle at the base of
35 the slab. At shallow depths (less than ~ 50 km) radiogenic heat produced in the crust
36 of the overriding plate and shear heating due to friction along the plate interface
37 can heat the top of the slab (e.g., Molnar and England, 1990; van Keken et al.,
38 2019). In most present-day subduction zones, the slab appears to remain decoupled
39 (over long geodynamical time scales) from the overriding mantle to a depth of 75–
40 80 km forming a “cold corner” in the mantle wedge (Furukawa, 1993; Wada and
41 Wang, 2009, Figure 1a). Below this depth the slab couples to the overriding mantle
42 wedge asthenosphere (Figure 1b). The motion of the subducting plate results in
43 a drag on the overlying mantle that leads to a cornerflow, which causes advective
44 transport of the hot mantle wedge material onto the slab that in turn provides
45 rapid warming of the slab surface and of the underlying oceanic crust and mantle
46 by further conduction.

47 The dramatic heating of the slab surface below the coupling depth (indicated
48 by d_c in Figure 1) is evident by the tightening of the isotherms near the slab surface
49 (Figure 1b) and the rapid heating of the slab surface (Figure 1c). While the oceanic
50 Moho (green line in Figure 1b) is only ~ 6 km from the top of the oceanic crust,
51 the temperature increase here is modest and lags significantly behind that at the
52 top. The average temperature gradient can be more than $50^\circ\text{C}/\text{km}$ throughout the
53 subducting crust. The conductive heat flow from the top is in competition with the
54 advective transport of the cold slab that originates at the trench. As a consequence,
55 one can predict that metamorphic reactions (including those involving dehydration)
56 occur at very different depths in the slab as it descends into the mantle.

57 Important primary factors that control the thermal conditions in subduction
58 zones at depth are the age of the incoming plate, the descent rate (which is con-
59 trolled by the convergence velocity at the trench and slab geometry), the frictional
60 properties of the shear zone decoupling the slab from the overriding plate, and, at
61 greater depth, the rheology of the mantle wedge that controls the corner flow. The
62 first two parameters are used in the subduction zone thermal parameter Φ which
63 is defined as the multiplication of age at the trench in Myr, convergence speed
64 in km/Myr, and the sine of the (average) dip of the slab geometry (Kirby et al.,
65 1996). The first two can be readily found for a given subduction zone section from
66 global databases (see approach discussed in Syracuse and Abers, 2006). The dip
67 dependence of Φ is useful if one wishes to estimate how fast the thermal effect of

68 subduction along a straight plane reaches a particular depth. Syracuse and Abers
69 (2006) determined the average dip for any of their 51 subduction zone segments by
70 averaging the dip within the 50 to 150 km depth contours (Ellen Syracuse, personal
71 communication). This approach was also used in determining the average dip for the
72 expanded selection of 56 subduction zone segments used in Syracuse et al. (2010).
73 It should be noted that this parameter is the most uncertain in Φ since it can
74 vary greatly depending on specific cross-section and the method used to determine
75 average dip. Since most subduction zones show a change from shallow dip at the
76 trench to intermediate or large dip at depth one should not be overly confident in
77 applying the thermal parameter – it might be more useful to consider a simplified
78 thermal parameter that is just age times convergence speed.

79 The thermal parameter (simplified or not) is a useful indicator whether we
80 might expect a subduction zone to be on the “warm” or “cold” end of the spectrum
81 or that it may be more “intermediate”. For example, using the Syracuse et al. (2010)
82 compilation, Cascadia ($\Phi=100$ km) and Nankai ($\Phi=450$ km) are by this criterion
83 among the warmest subduction zones whereas Tohoku and Hokkaido ($\Phi\sim 6000$ km)
84 and in particular Tonga ($\Phi=14,800$ km) are among the coldest. Cascadia and Tonga
85 occupy the extremes – the average and median values for Φ are 2900 km and
86 2200 km, respectively. It should be noted that the current value for Tonga is higher
87 than that in Syracuse and Abers (2006) who estimated $\Phi=6300$ km. The difference
88 is because Syracuse et al. (2010) took into account the addition of the high trench
89 retreat velocity due to the opening of the Lau backarc basin. An example that shows
90 a moderate correlation between Φ and slab temperatures at the top of the slab is in
91 van Keken et al. (2011, their Figure 2). By contrast, Figure 12F in Syracuse et al.
92 (2010) showed little correlation between the sub-arc slab surface temperature and
93 thermal parameter. There is no internal discrepancy here – the models used in these
94 two papers are largely similar. The reason for the scatter in the temperature at the
95 slab surface below the arc is that this part of the slab surface is still seeing a rapid
96 temperature increase due to the mantle wedge flow whereas at 120 km depth the
97 temperature increase is significantly more gentle (Figure 1c). This clearly suggests
98 that Φ in either of its forms should be used with caution when discussing processes
99 that occur below the arc.

100 1.2 Why do we need to know the thermal structure of subduction zones?

101 Before we start a discussion on how we can formulate subduction zone thermal
102 models it may be useful to consider why we might be interested in this in the first
103 place. We will provide a motivation by highlighting work from the last decade or
104 so that use model estimates from compilations of global models as presented, for
105 example, by Wada and Wang (2009) and Syracuse et al. (2010) to inspire exper-
106 iments or interpret geochemical and geophysical observations that are relevant to
107 our understanding of the dynamics of subduction zones. We embark on this section
108 with some trepidation as any conclusions and interpretations presented here may
109 only be as strong as the thermal models they are based on.

110 1.2.1 Design and interpretation of physical experiments

111 Global compilations of subduction thermal structure have been used extensively
112 to determine whether experimentally determined metamorphic changes and melt-
113 ing under various hydration states can occur in present-day subduction zones and

114 whether they can explain volcano geochemistry. For example, Tsuno et al. (2012)
115 determined that the sub-volcano slab surface below Nicaragua could not produce
116 carbonated sediment melting but that carbonitite production could occur in the
117 warmer overlying wedge after diapiric rise. Jégo and Dasgupta (2013, 2014) used
118 thermal model constraints to show that sulfur could be transferred from the slab to
119 mantle wedge either by aqueous fluids or by melting of the hydrated basaltic crust.
120 Brey et al. (2015) used global estimates to constrain experimental conditions of
121 carbonate melting in the presence of graphite or diamond. A similar approach was
122 taken by Merkulova et al. (2016) but now for studying the role of iron content on
123 serpentinite dehydration. Lee et al. (2021) used thermal models of cold subduction
124 zones to argue for the stability of chloritoid and its contribution to the relatively
125 strong trench-parallel seismicity observed in such regions.

126 Bang et al. (2021) used thermal models to study the stability of subducted
127 glaucophane over Earth's thermal evolution. Codillo et al. (2022) showed chlorite
128 is preferentially formed over talc during Si-metasomatism of ultramafic rocks while
129 also suggesting a limited rheological role of talc in determining the physical struc-
130 ture of subduction zones (as suggested to the contrary by Peacock and Wang, 2021).
131 Martindale et al. (2013) used models specific for the Marianas subduction zone to
132 design experiments focusing on high-pressure phase relations of volcanoclastic sedi-
133 ments and demonstrated that these sediments contribute widely to the geochemical
134 characteristics of Mariana arc magmas. The global spread of the predicted subduc-
135 tion zone thermal structures has also been used to understand the phase stability
136 field of various serpentinite phases and to rule out that a laboratory-produced high-
137 pressure form of antigorite could be stable inside the Earth (Reynard, 2013).

138 *1.2.2 Interpretation of geochemistry*

139 Thermal models have been used to interpret processes that contribute to geochem-
140 ical heterogeneity seen in arc lavas. Examples include those exploring the rela-
141 tionship between geochemical signatures of the subducting slab and arc volcanism
142 (Rustioni et al., 2021) as well as the mechanisms causing volcanism (Marschall and
143 Schumacher, 2012). Global models provided the suggestion that aqueous fluids and
144 hydrous melts produced enhanced chemical recycling particularly in hot subduction
145 zones (Hernández-Uribe et al., 2019). Applications to specific elemental or isotopic
146 systems include those of Ce and Nd under the Mariana volcanic arc (Bellot et al.,
147 2018) and the determination that nitrogen subduction in clay minerals is only pos-
148 sible in cold subduction zones (Cedeño et al., 2019). Slab surface temperatures
149 strongly correlate with Mg isotope ratios observed in volcanic arcs confirming a
150 thermal control on processes controlling Mg release from the subducting slab (Hu
151 et al., 2020). In a more regional example, slab surface temperatures in the Lesser
152 Antilles are predicted to be lower than that required for slab melting, suggesting the
153 role of dehydration of the slab crust (including sediments) as indicated for example
154 from K isotopic studies (Hu et al., 2021). Vho et al. (2020) used the average subduc-
155 tion zone thermal structure to model oxygen isotope variations to study fluid-rock
156 interaction. They suggested the potential for rapid serpentinization of the forearc
157 mantle by slab fluids and that the use of oxygen isotopes allows fluid pathways, the
158 type of flow, and pressure-temperature conditions encountered by the fluid to be
159 tracked.

160 Thermal models of the subducting slab such as those in van Keken et al. (2002)
161 and Syracuse et al. (2010) form a fundamental part of geochemical modeling appli-
162 cations facilitated by the Arc Basalt Simulator suite of tools (Kimura, 2017; Kimura
163 et al., 2009). A few examples of the many applications of these tools are as follows.
164 Mazza et al. (2020) found that the slab thermal structure controls release of tung-
165 sten and its isotopic ratios which allows for tracing of slab dehydration and slab
166 melting. Kimura et al. (2014) showed that the wide diversity of magma types found
167 through SW Japan in response to the subduction of the young Philippine Sea Plate
168 was caused by melting of the slab and that this induced flux melting of peridotite
169 in the mantle wedge. A combined geochemical and geophysical study explored the
170 role of water in magma genesis in the much colder NE Japan subduction zone and
171 allowed for mass balance constraints on local water fluxes (Kimura and Nakajima,
172 2014). Variations of arc lava composition between the volcanic arc and backarc in
173 the northern Izu arc could be explained by differences in the pressure and tempera-
174 ture conditions during melting in addition to variable water content (Kimura et al.,
175 2010).

176 *1.2.3 Translation of mineral physics to geophysical quantities*

177 Slab thermal models are routinely used in interpreting how the presence of volatiles
178 could affect geophysical properties predicted from laboratory experiments (e.g.,
179 Förster and Selway, 2021; Huang et al., 2021; Pommier et al., 2019). This allows
180 for the interpretation of the role of fluids in explaining electromagnetic and magne-
181 totelluric observations over subduction zones (Förster and Selway, 2021; Pommier
182 and Evans, 2017). Chen et al. (2018) used thermal model predictions for various
183 regions to understand the role of phengite dehydration on the formation of high
184 conductivity anomalies above subducting slabs. Similar studies focused on the in-
185 fluence of dehydration on the electrical conductivity of epidote (Hu et al., 2017),
186 talc (Wang et al., 2020), NaCl-bearing aqueous fluids (Guo and Keppeler, 2019), and
187 glaucophane (Manthilake et al., 2021).

188 *1.2.4 Plate interface earthquakes, slow slip, and episodic tremor*

189 Global thermal models have also been used to explore seismic processes occurring at
190 the plate interface below the forearc, which include the seismogenic zone that expe-
191 rience underthrusting seismic events (such as the 2011 Tohoku-oki earthquake) that
192 are separated by interseismic periods. Understanding the rheological properties of
193 the plate interface, for example whether the plate interface is locked or deforms by
194 aseismic creep (see, e.g., Loveless and Meade, 2011), is essential to understand the
195 seismic hazards in a particular subduction zone. The discovery of episodic tremor
196 and slip (e.g., Rogers and Dragert, 2003) and its relation to low-frequency earth-
197 quakes (Shelly et al., 2006) has led to a further appreciation of the important role of
198 rheology and fluid production along the plate interface. These processes are both at
199 least in part temperature-dependent and it is expected that various features of the
200 plate interface are controlled by the thermal characteristics of a given subduction
201 zone. As an example, use of specific thermal models showed a relatively low tem-
202 perature (less than 300°C) at the down-dip limit of the seismogenic zone (Fagereng
203 et al., 2018). In a study combining field examples of sand-shale mélanges from Ko-
204 diak accretionary complex and the Shimanto belt with kinematic modeling, Fisher

205 et al. (2019) demonstrated the strong influence temperature at the slab top has on
206 the healing of cracks that modulate the fault zone strength during the interseismic
207 period. The Syracuse et al. (2010) model for Tohoku was used as a basis for models
208 explaining the viscoelastic flow after the 2011 Tohoku-oki earthquake (Agata et al.,
209 2019). Condit et al. (2020) showed from warm subduction zone models that locally
210 produced fluids are sufficient to explain episodic tremor and slip events.

211 *1.2.5 Nature of intermediate-depth and deep seismicity*

212 Earthquakes in the shallow crust and mantle as well as underthrusting events along
213 the seismogenic zone tend to be caused by brittle failure, which is possible due to dif-
214 ferential stresses under modest hydrostatic pressures. At depths greater than ~ 40 -
215 70 km the hydrostatic pressure becomes large enough to make brittle failure ineffec-
216 tive, which therefore requires different physical mechanisms to cause intermediate-
217 depth (~ 70 -400 km) and deep (~ 400 -700 km) earthquakes (see Frohlich, 2006).
218 Intriguingly, intermediate-depth seismicity seems to have a strong petrological con-
219 trol as shown by Abers et al. (2013). In cold subduction zones such as Tohoku and
220 Hokkaido the upper plane seismicity of the Wadati-Benioff zone peaks in the oceanic
221 crust (Figure 2a). The oceanic crust in warm subduction zones tends to have little
222 seismicity in the oceanic crust with seismicity peaking in the slab mantle (Figure
223 2b). Abundant seismicity and dense seismic networks allow for precise hypocenter
224 locations below Japan (e.g., Kita et al., 2010b). Thermal modeling suggests that
225 the major dehydration reaction of blueschist to lawsonite eclogite facies (informally
226 denoted as the “blueschist-out” boundary; Figure 2c) occurs at a pressure and tem-
227 perature range just where seismicity in the upper plane disappears (van Keken
228 et al., 2012, Figure 2d). This strongly suggests that fluids caused by dehydration
229 of blueschist facies rock travel back up the slab triggering the shallower seismic-
230 ity, possibly through hydrofracturing caused by fluid overpressure (Padrón-Navarta
231 et al., 2010). The presence of free fluids in parts of the oceanic crust below Tohoku
232 that have abundant seismicity is strongly suggested from observations of very low
233 P-wave speeds in seismically active region of the subducting crust below Tohoku
234 (Shiina et al., 2013, Figure 2e) and Hokkaido (Shiina et al., 2017).

235 Sippl et al. (2019) interpreted the seismicity distribution in the Northern Chile
236 subduction zone to be caused by the production of fluids due to metamorphic de-
237 hydration reactions triggered by heating when the slab gets into contact with the
238 hot mantle wedge. In this region, Bloch et al. (2018) demonstrated a correlation
239 between earthquakes and a high V_p/V_s region in the lower plane of the double seis-
240 mic zone that is likely due to antigorite dehydration at depth and the presence of
241 fluids at shallower depths. Wei et al. (2017) showed that the double seismic zone in
242 Tonga extends to a maximum depth of 300 km with a clear trend of the maximum
243 depth along a given profile correlating with the convergence speed, suggesting that
244 metamorphic dehydration, likely that of antigorite, occurs when the slab interior
245 first reaches $\sim 500^\circ\text{C}$.

246 Independent support for the role of free fluids in the subducting oceanic crust
247 is provided by modeling of fluid flow in subduction zones where the (important,
248 but often ignored) driving force of pressure gradients caused by compaction of rock
249 upon dehydration is included. Without this force fluids tend to leave the slab by

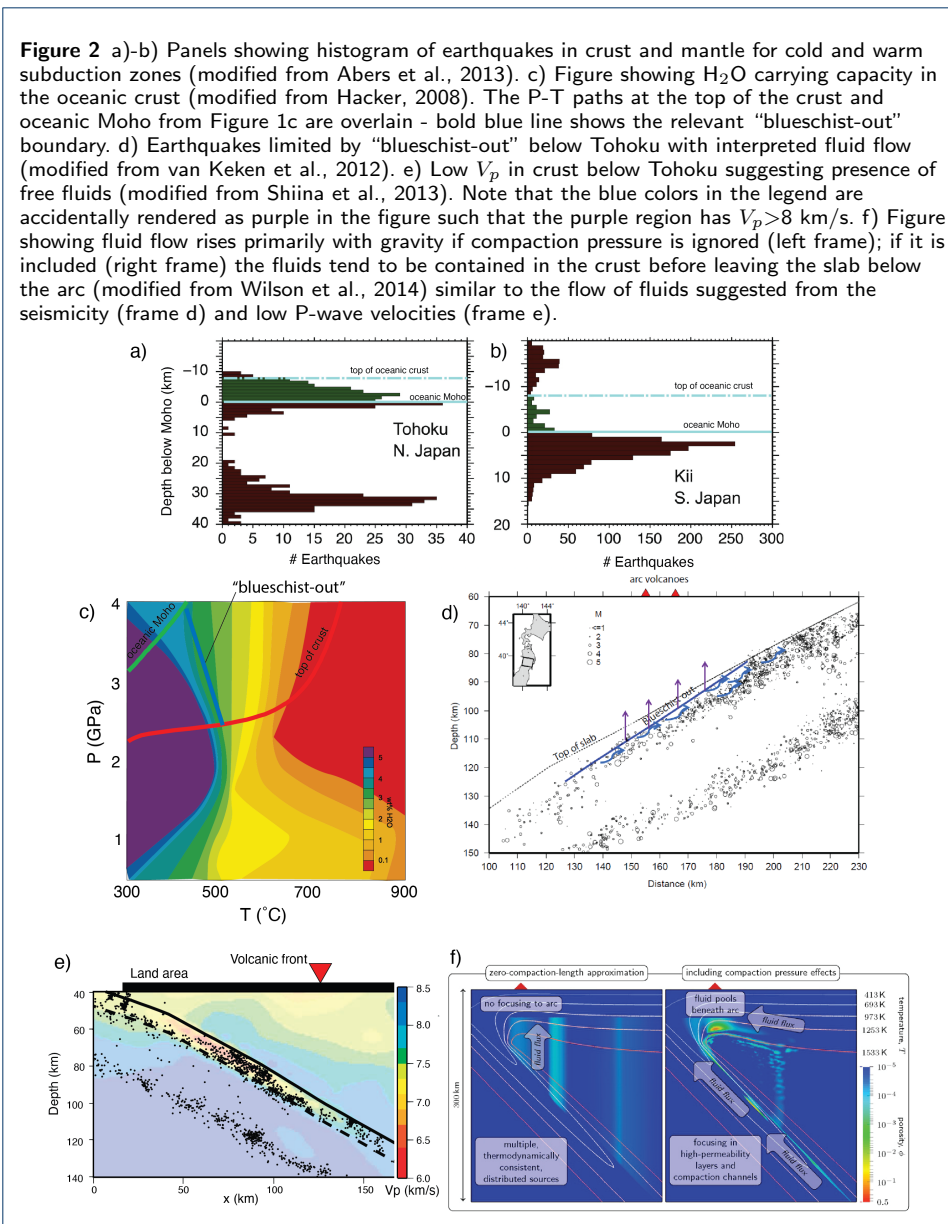
250 buoyancy alone – with compaction pressure fluids released by dehydration reactions
251 in the crust tend to travel back up the subducting crust before exiting the slab
252 (Wilson et al., 2014, Figure 2e). Note that the model with compaction pressure
253 causes the fluids to exit below the arc allowing for a self-consistent explanation of
254 the location of the arc. The broad and distributed fluid release from the slab in the
255 buoyancy-only model would predict multiple volcanic fronts which is generally not
256 observed. The suggestion that distributed seismicity is caused by fluid flow in the
257 slab is an alternative to ideas presented by Ferrand (2019) who used various thermal
258 model estimates of the pressure-temperature conditions in earthquake hypocenters
259 to argue that dehydration of antigorite as well as other hydrous phases causes
260 stress transfer to trigger seismicity. It should be noted that pervasive fluid flow is
261 also evident from field observations of exhumed portions of the oceanic crust (e.g.,
262 Bebout and Penniston-Dorland, 2016; Piccoli et al., 2016).

263 Fluids may also play a critical role in deeper seismicity which forms an alterna-
264 tive to proposed processes such as shear heating instabilities (Kelemen and Hirth,
265 2007; Prakash et al., 2023). For example, Shirey et al. (2021) explored the corre-
266 lation between seismicity, dehydration reactions, and diamond formation in cold
267 subduction zones. They argued from thermal modeling that the conditions for deep
268 intermediate-depth seismicity are principally met in cold subduction zones because
269 in these regions the crust and uppermost mantle can bypass shallow dehydration
270 reactions.

271 Note that seismicity in the subducting slab is generally widely distributed
272 rather than tightly clustered. This appears to be in conflict with the hypothe-
273 sis that embrittlement due to mineral dehydration reactions is the main cause for
274 intermediate-depth seismicity (e.g., Jung et al., 2004; Raleigh and Paterson, 1965).
275 Dehydration embrittlement would cause earthquakes to be located at the site of de-
276 hydration reactions that are in a narrow pressure-temperature range and therefore
277 would cause clustering of earthquakes around these boundaries which is contrary
278 to observations (see also Ferrand, 2019). While heterogeneity, such as the variable
279 presence (and absence) of hydrous phases would create patches rather than (near-
280)continuous seismicity but this would still occur under specific pressure-temperature
281 conditions if dehydration embrittlement were the main mechanism and would there-
282 fore not explain the widely distributed seismicity.

283 *1.2.6 Mobilization and deep cycling of volatiles*

284 Compilations of thermal subduction zone structures have been critically used (along
285 with predictions of metamorphic phase stability and water content as a function of
286 lithology, pressure, and temperature) to understand where fluids are being released
287 from the slab (Cannaò et al., 2020; Hermann and Lakey, 2021; Rüpke et al., 2004;
288 van Keken et al., 2011; Vitale Brovarone and Beyssac, 2014). This applies particu-
289 larly to the release of H₂O but also to that of carbon by aqueous fluids (Arzilli
290 et al., 2023; Farsang et al., 2021). Tian et al. (2019) used simplified models of
291 thermal structure with a comprehensive thermodynamic parameterization of open
292 system reactive flow in the subducting slab. They showed the importance of redis-
293 tribution of carbon by fluid flow within the lithological layers and that the subduc-
294 tion efficiency of H₂O and CO₂ is increased by fractionation within the subducting



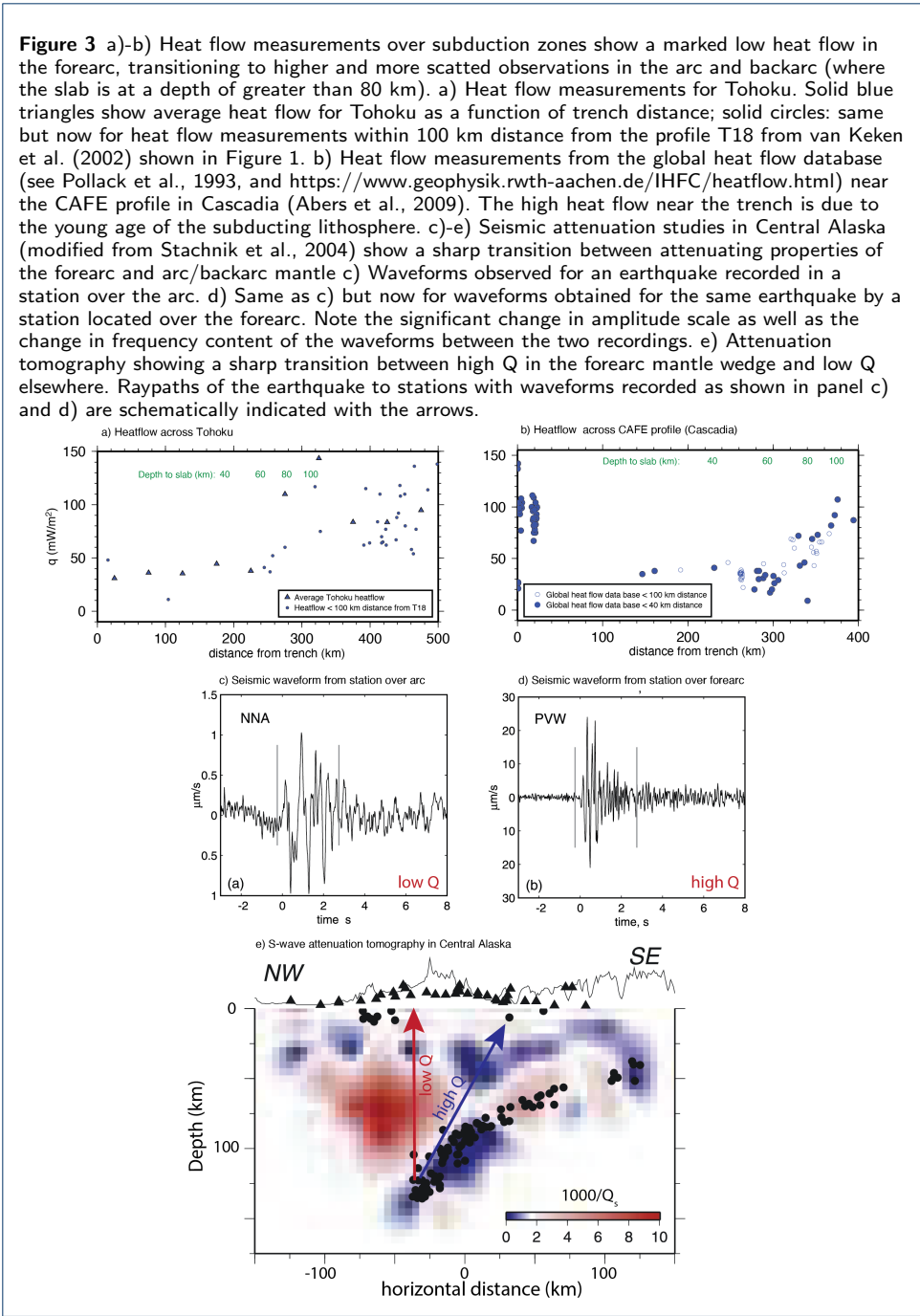
295 lithologies. These approaches not only facilitate our understanding of the release
 296 of fluids and their contribution to subduction zone processes, but also have been
 297 used as input to global models predicting the long term chemical evolution of the
 298 Earth’s mantle (e.g., Kimura et al., 2016; Shimoda and Kogiso, 2019). In a separate
 299 study, Smye et al. (2017) used the global set of thermal models to quantify noble
 300 gas recycling into the deep mantle. They showed a correlation between noble gases
 301 and H₂O and that strong fractionation occurred in warm subduction zone settings
 302 with minimal fractionation in cold slabs.

303 **2 Geophysical observations guiding modeling of the thermal** 304 **structure of subduction zones**

305 Figure 1a provides a cartoon of subduction zone structure that builds on geophys-
306 ical observations of heat flow, seismology, and geodetics. Combined, these methods
307 indicate that the mantle wedge is composed of a hot region below the arc and
308 backarc that is fairly sharply delineated from a cold forearc mantle in the tip of the
309 wedge where the slab surface is above ~ 80 km depth. This wedge tip has generally
310 been called the “cold corner” or “cold nose” of the mantle wedge that indicates
311 the presence of significant rheological heterogeneity of the slab surface and mantle
312 wedge that directly controls the thermal structure of subduction zones (and can
313 therefore be used to construct thermal models such as the one in Figure 1b). In
314 this section we will explore the main geophysical observations that have led to the
315 concept of the “cold nose” and the partitioning of the mantle wedge into a cold and
316 hot region that is separated by a fairly sharp vertical boundary.

317 **2.1 Heat flow**

318 Early heat flow measurements in the Tohoku subduction zone (see discussion and
319 citations in Honda, 1985) suggested a significant change in heat flow values when
320 moving from the trench to the volcanic arc – very low heat flow values over the
321 forearc are sharply separated from much higher and more scattered heat flow val-
322 ues in the arc and backarc. The scattered values in the arc and backarc regions are
323 likely due to local processes such magma transport in the crust and heterogeneous
324 heat production, as well as potential bias in the continental data (Furukawa and
325 Uyeda, 1989). An updated heat flow database for Japan (Tanaka et al., 2004) shows
326 broad consistency of this pattern along Tohoku and Hokkaido (Figure 3a). Simi-
327 lar observations are now available for many subduction zones, including the Andes
328 (Henry and Pollack, 1988; Springer and Förster, 1998), Cascadia (see compilation
329 in Currie et al., 2004, and Figure 3b), Kermadec (Von Herzen et al., 2001), and
330 Ecuador–Columbia (Marcaillou et al., 2008). Heat flow data are traditionally ob-
331 tained using Fourier’s law by measuring the thermal gradient and rock conductivity
332 in boreholes (Pollack et al., 1993) or by marine heat flow probes (e.g., Hyndman
333 et al., 1979). Alternative methods employ electromagnetic measurements of the
334 Curie point depths and seismic observations of the Bottom-Simulating Reflector
335 (BSR). The first method makes use of change from ferromagnetic to paramagnetic
336 behavior in minerals such as magnetite when rock is heated above the Curie tem-
337 perature. Determining the depth of this transition therefore allows for estimates
338 of the average thermal gradient in the crust with examples in Mexico (Manea and
339 Manea, 2011), northeast Japan (Okubo and Matsunaga, 1994) and the western Pa-
340 cific (Yin et al., 2021). The second method measures the location of the base of
341 the stability field of clathrate hydrates which has a well-calibrated temperature and
342 pressure range. Depth determinations of the BSR lead therefore to determinations
343 of temperature gradients and from that estimates for the average heat flow through
344 the shallow crust. Examples of the application of the BSR technique exist for Cas-
345 cadia (Salmi et al., 2017), Costa Rica (Harris et al., 2010), Hikurangi (Henry et al.,
346 2003), and Nankai (Hyndman et al., 1992; Ohde et al., 2018).



347 2.2 Seismology

348 Seismological methods provide critical information on the geometry of the sub-
 349 ducting slab and structure of the overlying mantle wedge. For example, teleseismic
 350 determinations of intermediate-depth and deep seismicity in Wadati-Benioff zones
 351 have been used to delineate the position of subducting slabs (Gudmundsson and
 352 Sambridge, 1998). Important improvements over these early models include earth-
 353 quake hypocenter relocation using global tomographic models (e.g., Portner and
 354 Hayes, 2018; Syracuse and Abers, 2006). Additional information can be obtained

355 from active-source seismic studies, local seismicity catalogs, and the use of PS and
356 SP converted phases at velocity interfaces that may provide information about the
357 location of the Moho or the top of the subducting crust (Bostock, 2013; Kim et al.,
358 2021; Zhao et al., 1994). The most recent and comprehensive global slab surface ge-
359 ometries using a combination of these techniques is provided by Hayes et al. (2018).
360 Local earthquake conversions (Shiina et al., 2013) and guided-wave studies (e.g.,
361 Abers et al., 2006; Rondenay et al., 2008) provide information on the hydration
362 state of the subducting crust which can further constrain thermal models.

363 Observations of seismic attenuation (which is a measure of the absorption of
364 seismic energy by non-elastic processes) is highly sensitive to temperature (Faul and
365 Jackson, 2005; Takei, 2017) and can be used to map out in particular the hot re-
366 gions in subduction zones. Commonly observed features are a low attenuation slab
367 dipping below a high attenuation mantle wedge. Seismic attenuation is quantified
368 by the quality factor Q which is inversely proportional to the degree of attenuation.
369 It has been a common and long-standing observation (e.g., Sacks, 1968; Utsu, 1966)
370 that waveforms from local earthquakes tend to have higher frequency and higher
371 amplitude characteristics when they are observed by stations in the forearc com-
372 pared to those observed in the arc and backarc (Figure 3c,d). In many regions it
373 has now become possible to map out the attenuation structure in subduction zones
374 in enough detail to see clear evidence of the cold corner with often a sharp, near-
375 vertical boundary separating the nose of the wedge down to a slab depth of 75–80 km
376 from the strongly attenuating mantle wedge below the arc and back-arc. Such re-
377 gions include Peru (Jang et al., 2019), New Zealand (Eberhart-Phillips et al., 2020),
378 the Lesser Antilles (Hicks et al., 2023), Tohoku (Nakajima et al., 2013), Nicaragua
379 (Rychert et al., 2008), Central Alaska (Stachnik et al., 2004, Figure 3e), Ryukyu
380 (Ko et al., 2012), the Aegean (Ventouzi et al., 2018), Tonga (Wei and Wiens, 2018),
381 and the Marianas (Pozgay et al., 2009). In contrast, a 3D attenuation study of the
382 Kyushu subduction zone showed low Q in the forearc mantle (Saita et al., 2015)
383 which the authors contributed to a relatively high degree of serpentinization.

384 A weak and partially inverted Moho in Cascadia (Bostock et al., 2002; Brocher
385 et al., 2003; Hansen et al., 2016) further illustrates the unusual nature of the forearc
386 mantle. The crust-mantle interface is generally seen as a strong velocity contrast
387 with a change from low crustal velocities to higher mantle velocities. This is the
388 case in the backarc of Cascadia, but the near disappearance of the Moho and partial
389 inversion below the forearc here suggests that the underlying mantle wedge has
390 a lower seismic velocity than the ambient mantle. Extensive serpentinization has
391 been suggested as main cause for this velocity change (Bostock et al., 2002) but
392 the change could also be due to the gabbroic nature of the overlying Siletzia terrain
393 (Crosbie et al., 2019). Low V_p velocities in the cold corner seem to be largely limited
394 to Cascadia (Abers et al., 2017). This is likely due to the less efficient dehydration
395 of the slab (and limited sourcing of fluids to the overlying forearc mantle wedge) in
396 most other, colder, subduction zones (van Keken et al., 2011).

397 Of further note, particularly for subduction zones in northeastern Japan and
398 Ryukyu, is a marked transition in SKS splitting between forearc and arc (e.g., Long
399 and van der Hilst, 2005; Nakajima and Hasegawa, 2004). This has been interpreted
400 by some to represent B-type olivine fabric in the cold, moderately hydrated, and

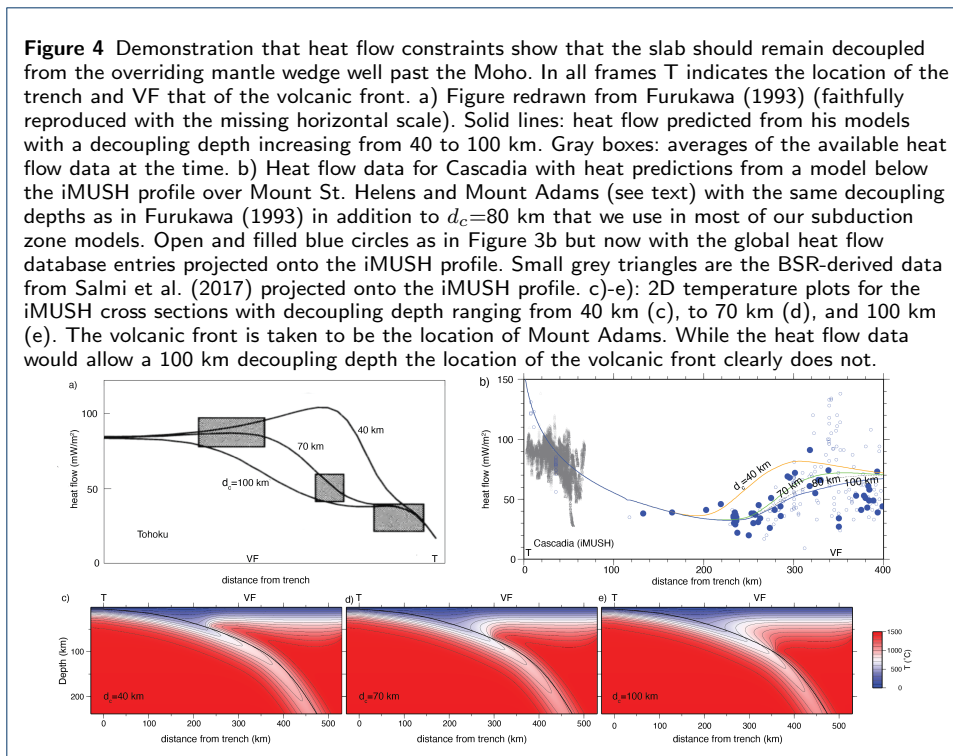
401 relatively high-stress cold corner (Kneller et al., 2007; Long and van der Hilst,
402 2006). It could alternatively be due to the crystal-preferred orientation formed by
403 deformation of serpentine (e.g., Brownlee et al., 2013; Horn et al., 2020; Katayama
404 et al., 2009; Mookherjee and Capitani, 2011; Nagaya et al., 2016; Wang et al., 2019)
405 or perhaps is caused by a combination of these two mechanisms (Kneller et al., 2008;
406 McCormack et al., 2013). Wang et al. (2019) also demonstrated clear evidence of
407 the slab-mantle decoupling depth from anisotropic imaging. Of note here is the
408 anisotropy observed from SKS splitting in Central Alaska, with a marked shift in
409 direction of splitting, but now from trench-normal in the forearc and trench-parallel
410 in the arc and backarc region (Christensen and Abers, 2010). It should be noted
411 that the idea of slow convection with weak fabric development in the forearc of the
412 northeastern Japan subduction zone may need revision given new off-shore seismic
413 evidence that the forearc here may be stagnant and that the weak trench-parallel
414 anisotropy originates from pre-existing fabric in the subducting crust (Uchide et al.,
415 2020).

416 2.3 Geodetics

417 An intriguing new approach to physically map the extent and properties of the cold
418 corner is through the use of postseismic deformation following large seismic events.
419 Forward modeling can be used to constrain the differences in rheological behav-
420 ior between a mostly elastic forearc mantle compared to the visco-plastic arc and
421 backarc. This became a focus in modeling studies of the aftermath of the Tohoku-oki
422 earthquake that took into account the properties of the Pacific slab. Such models
423 require a thermal structure with a cold forearc separated from a warm arc region
424 similar to that suggested from heat flow and seismology as described above (Freed
425 et al., 2017; Hu et al., 2014; Luo and Wang, 2021; Muto et al., 2016, 2019). A useful
426 review of this evolution in thought is in Dhar et al. (2023). Alternative models that
427 focused primarily on temperature-dependent rheology also require a similar thermal
428 structure to fit postseismic uplift data (e.g., Peña et al., 2020; van Dinther et al.,
429 2019). Dhar et al. (2022) used a newly deployed geodetic network to demonstrate
430 along-arc variations in the structure of the cold nose, with a narrowing of the nose
431 below Miyagi and a broadening below Fukushima.

432 2.4 The cold corner requires mechanical decoupling between the slab and shallow 433 mantle wedge

434 The geophysical evidence presented above requires the presence of a cold corner in
435 the mantle wedge. This in itself requires that this part of the wedge is mostly isolated
436 from the convective cornerflow and that therefore the slab remains decoupled below
437 the seismogenic zone to a depth of 75–80 km. The geophysical data also require a
438 relatively sharp transition to full slab-wedge coupling below this depth. In Figure 4
439 we reevaluate the classical models by Furukawa (1993) for the Cascadia subduction
440 zone. The model is similar to the Cascadia model in Syracuse et al. (2010) but
441 has been modified for the geometry, convergence velocity, and age at the trench
442 of the slab below the imaging Magma Under mount St. Helens (iMUSH) array
443 (Mann et al., 2019). In this model we also take into account the low radiogenic
444 heat production in the continental crust due to the gabbroic nature of the accreted



445 Siletzia terrane (Wells et al., 2014), which explains the very low heat flow in the
 446 forearc region (Figure 4b). The models are more fully described in Pang et al.
 447 (2023) and are available in the Supplementary Information (see data availability
 448 statement). These models show that heat flow and position of the volcanic arc are
 449 not satisfied by a very shallow (40 km) or deep (100 km) decoupling point, but that
 450 a depth of around 70–80 km gives satisfactory model results. Other examples are
 451 in Wada and Wang (2009).

452 We will not delve deeply into the very interesting question of why this decoupling
 453 seems to end at that depth but one can find abundant interest and suggestions
 454 for potential causes in the literature. Proposed mechanisms and features include the
 455 presence of weak phases such as serpentinite (Burdette and Hirth, 2022; Wada et al.,
 456 2008), the role of secondary phases (Peacock and Wang, 2021), or the convolution
 457 of multiple competing effects (Kerwell et al., 2021). It should be noted that ex-
 458 planations that rely on dehydration reactions that are largely isothermal at 2–4
 459 GPa (such as those of antigorite and chlorite) lead to dynamics that are difficult to
 460 reconcile with a fixed-depth transition (see, e.g., the T550 models in Syracuse et al.,
 461 2010). Note also that the weak nature of antigorite has been recently questioned
 462 using experiments that showed stronger, semi-brittle deformation under relevant
 463 forearc conditions (Hirauchi et al., 2020).

464 We will in the remainder of this pair of papers assume that the slab is decoupled
 465 from the overriding crust and mantle to a depth of 80 km at which point it couples
 466 to and drags down the overriding mantle wedge (Figure 1). We will then explore
 467 the resulting effects on the thermal field in subduction zones and compare these to
 468 observations.

469 **3 Selected literature examples of numerical models exploring** 470 **subduction zone thermal structure**

471 In wrapping up part I of this review paper we will highlight a few modeling studies.
472 The literature covering approaches to understand and use the thermal structure
473 of subduction zones through modeling is vast and cannot be covered fully in an
474 introductory review. To limit our present scope we will focus on literature that was
475 published in the last decade or so and that studies the thermal structure of the
476 Japanese subduction systems in particular.

477 **3.1 Why Japan?**

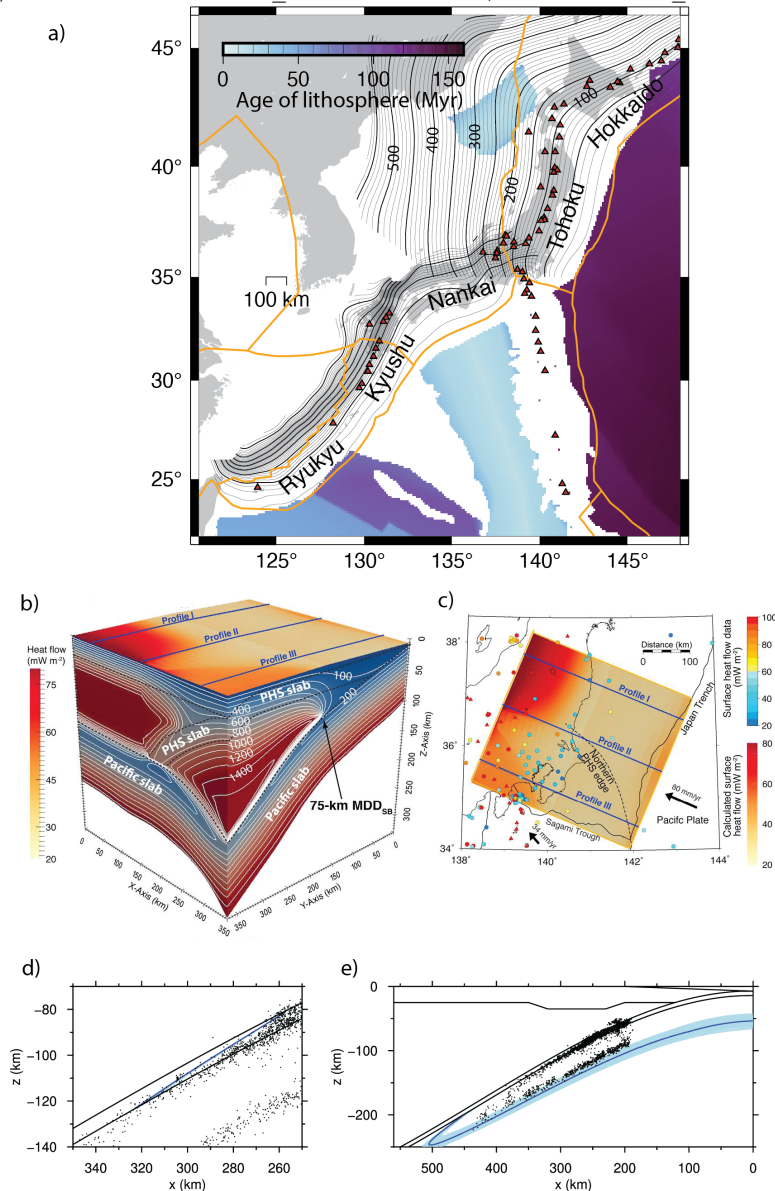
478 Subduction zones in Japan (Figure 5a) are predicted to have a broad range of
479 thermal structure with the thermal parameter ranging across more than an order of
480 magnitude, from the relatively slow subduction of the young Philippine Sea Plate in
481 Nankai (thermal parameter $\Phi=450$ km) to fast subduction of old oceanic lithosphere
482 in NE Japan ($\Phi=5100-6000$ km), with intermediate conditions for Ryukyu and
483 Kyushu ($\Phi=1600-2100$ km). An introductory tour of thermal models of this region
484 will therefore provide us with an efficient and focused way of exploring the features
485 that may characterize the global subduction system.

486 **3.2 Nankai**

487 The shallow structure of the Nankai subduction zone is of particular interest to
488 understand the mechanisms leading to large underthrusting events and the role
489 of low frequency earthquakes, tectonic tremors, and slow slip. Harris et al. (2013)
490 complemented a synthesis of the extensive off-shore heat flow measurements with
491 2D thermal modeling to show that heat flow data suggest pervasive fluid flow in
492 the oceanic crust. This leads to differences in estimates of temperature along the
493 seismogenic zone of up to 100°C compared to models that do not take this fluid
494 flow into account. Hamamoto et al. (2011) also combined heat flow data and 2D
495 thermal modeling to show that the shear stress on the plate interface in the central
496 part of the Nankai Trough is very low. Using the, at the time, most recent heat flow
497 data, Yoshioka et al. (2013) demonstrated, using thermal models along a number
498 of 2D cross sections, the importance of shear heating along the plate interface and
499 that the thermal effects of surface erosion and sedimentation due to Quaternary
500 deformation has to be taken into account. Suenaga et al. (2019) performed 2D
501 thermal modeling to show that the metamorphic phase change from amphibolite
502 to eclogite with its associated fluid release controls the location of low-frequency
503 earthquakes and tectonic tremors.

504 A combination of features makes the Nankai subduction zone very challenging
505 for thermal modeling. These include: relative recent (re)initiation of subduction of
506 the Philippine Sea Plate into a region of mature subduction of the Pacific below NW
507 Japan; the complicated and time-variable tectonic history (Kimura et al., 2005);
508 the variable age of the incoming lithosphere (e.g., Seno and Maruyama, 1984);
509 and changes in apparent dip along-strike (see discussion in Wang et al., 2004). In
510 addition, the proximity of the Euler pole between the Philippine Sea Plate and the
511 Eurasian plate (Seno, 1977) causes oblique convergence with changes of obliquity
512 along strike. This suggests that we can draw the most confidence from models

Figure 5 a) Map of the Japanese subduction systems. Black contours show depth to the top of the subducting slab (from Hayes et al., 2018) for the Japan, Nankai, Kyushu, and Ryukyu segments at 10 km intervals (50 km intervals are in bold). Red triangles show locations of arc volcanoes. Orange lines are plate boundaries from Bird (2003). Age of oceanic lithosphere is from Müller et al. (2008). b) 3D model showing subduction of the Philippine Sea Plate (PHS) and Pacific slab below the Kanto region (modified from Wada and He, 2017). MDD=maximum decoupling depth (denoted as d_c in this paper). c) Heat flow comparison between observations (Tanaka et al., 2004) and model predictions (also modified from Wada and He, 2017). d) Predicted “blueschist-out” boundary below Tohoku (modified from Morishige, 2022) assuming this occurs, as in van Keken et al. (2012), at $T=617-52P$ (in °C with P in GPa). Compare with Figure 2b. e) as frame d) but now for the serpentinite-out boundary using, as in Faccenda et al. (2012), $T=740-1.8P-3.9P^2$ at $P \geq 2.1$ GPa and $T=478+180P-31P^2$ at $P < 2.1$ GPa.



513 that are 3D, time-dependent, and take time-dependent changes in the age of the

514 incoming slab and convergence parameters into account. Such studies are, aside
515 from complicated, quite expensive computationally but there are a few such studies
516 that we can highlight. Ji et al. (2016) showed that the changes in obliquity caused
517 significant variations in temperature along the plate interface providing a potential
518 example for lateral changes in the occurrence of low-frequency earthquakes and slow
519 slip events. Morishige and van Keken (2017) focused on changes in curvature of the
520 slab and suggested that focused fluid migration explains along-strike differences in
521 accumulated slip rates of slow slip events. Wada and He (2017) focused on the
522 interaction between the recently subducting Philippine Sea plate into the mature
523 subducting of the Pacific below the Kanto region (Figure 5b). This study confirmed
524 that the heat flow data were best explained by a decoupling depth of 75 km here
525 (Figure 5c). Given the relatively young age of the Nankai subduction zone this
526 study suggests the characteristics of the plate interface that lead to the cold corner
527 establishes early. They also found that the down-dip limit of the seismogenic zone
528 is characterized by the 350°C isotherm throughout the region.

529 3.3 Tohoku and Hokkaido

530 For a thermal modeler, the relatively uniform subduction of the old Pacific litho-
531 sphere below NW Japan provides a welcome respite from the complications in
532 Nankai. Convergence becomes somewhat oblique when moving north from the Japan
533 Trench to the Kurile Trench but convergence characteristics vary relatively little
534 along strike.

535 Extending the suggestion by Kita et al. (2010b), van Keken et al. (2012) demon-
536 strated that the uppermost seismicity contained within ~ 7 km from the slab top is
537 controlled by metamorphic dehydration reactions in the subducting oceanic crust by
538 showing that, to reasonable confidence, this seismicity disappears at the blueschist-
539 out dehydration reaction across most of the Tohoku-Hokkaido subduction zone. An
540 important exception was for a cross-section across SW Hokkaido. Below this region
541 the seismic belt deepens anomalously which was suggested to be caused by the
542 thermal effects of subducted forearc crust (Kita et al., 2010a). Using 2D model-
543 ing, van Keken et al. (2012) failed to confirm this hypothesis and suggested that
544 3D flow caused by geometrical changes at the junction of the Tohoku-Kurile arc
545 (as demonstrated by Morishige and Honda, 2013) may be the real cause for the
546 anomalous characteristics of upper plane seismicity here. Using 3D thermal mod-
547 eling Morishige and van Keken (2014) provided a negative test of this hypothesis.
548 They showed that the thermal variations caused by 3D flow were too small to ex-
549 plain the deepening of the seismic belt. By contrast, Wada et al. (2015) were able to
550 show a significant cooling of the mantle wedge at the transition between the Tohoku
551 and Hokkaido subduction zones potentially because they used a more realistic slab
552 geometry than the idealized one in Morishige and van Keken (2014). Wada et al.
553 (2015) also cautioned that the cooling effect they predicted might be an overes-
554 timate due to the assumption of steady state. This suggests that the anomalous
555 character of subduction below SW Hokkaido remains an important topic for future
556 research.

557 The Tohoku subduction zone was the focus in a study by Morishige (2022) to
558 test whether variable thermal properties (such as thermal conductivity and thermal

expansivity) could have a significant effect on the thermal structure of the subducting slab. A novel aspect of this study was the use of a Bayesian inversion to make sure the thermal structure of the incoming plate satisfied constraints from heat flow and bathymetry. The conclusion of this study was that one could use constant thermal properties since differences in thermal structure between these two assumptions were found to be small. It confirmed the importance of the blueschist-out boundary on controlling the depth of the upper belt of seismicity (Figure 5d) and showed that the lower plane of the double seismic zone was in the serpentinite stability field (Figure 5e), confirming earlier suggestions that the deeper plane seismicity might be related to the production of fluids by metamorphic dehydration of the slab mantle (e.g., Faccenda et al., 2012; Hacker et al., 2003; Peacock, 2001).

Horiuchi and Iwamori (2016) explored fluid release and flow in the mantle wedge below Tohoku. They showed they could to a reasonable degree match observations of the location of the volcanic arc, seismic tomography, and heat flow if the initial water content of the incoming slab was 2–3 wt% and the viscosity of the modeled serpentinite layer was in the range of 10^{20} – 10^{21} Pa·s. Yoo and Lee (2023) provided a similar study of fluid production and release along with melt generation and freezing. They suggested that the observed melt focusing below the Tohoku volcanic arc can be best explained by a relatively deep decoupling depth (90 km) with an important role for melt freezing.

3.4 Kyushu and Ryukyu

The Kyushu and Ryukyu subduction zones are characterized by faster (~ 7 cm/yr), more mature, and steeper subduction of somewhat older (27–43 Myr) lithosphere compared to Nankai. These subduction zones have a northern termination at the Kyushu-Palau ridge and end to the south at Taiwan.

There are a few studies of note in this region that particularly focused on constraining thermal conditions from the seismic characteristics of the plate interface. Thermal modeling showed that lateral variations in the characteristics of short-term slow slip events in Ryukyu could not be explained by thermal variations alone, but could be due to variable fluid flux from the oceanic crust (Suenaga et al., 2021). Gutscher et al. (2016) used 2D thermal models near the southern termination of the Ryukyu subduction zone combined with the characteristics of the seismogenic zone to argue either for a thermal rejuvenation of the westernmost Philippine Sea Plate or that toroidal flow in the mantle wedge caused warmer than expected conditions here (see also the discussion in part II about 3D flow effects on thermal structure). Using a 2D model for Kyushu that matched local heat flow data, Suenaga et al. (2018) showed that tectonic tremors occurred in the mantle wedge corner at temperatures between 450–650°C and that the afterslip of the 1996 Hyuga-nada earthquake occurred where the plate interface is at 300–350°C. This is at the high end of temperatures suggested for the seismogenic zone (Hyndman et al., 1995) suggesting therefore that maximum afterslip occurred near the down-dip end of the seismogenic zone in their model.

4 Conclusions for Part I

We provided the motivation for the need to understand the thermal structure through geodynamical modeling and provided a select number of examples of such

604 models. In part II we will turn to explore numerical methods that can be used to
 605 model this thermal structure, provide ways to test the quality of such models, and
 606 provide a comparison between model predictions for subduction zone temperatures
 607 and observations of these from geochemical and geophysical observations.

608 **Availability of data and material**

609 All geophysical and geochemical data and all modeling studies presented (except those in frames b through e of
 610 Figure 4) are taken from the literature. Modelled temperature and heat flow for Figure 4 (frames b through e) are
 611 available via the Zenodo repository doi.org/10.5281/zenodo.7843967.

612 **Competing interests**

613 The authors declare that they have no competing interest.

614 **Funding**

615 No funding was obtained for this study.

616 **Authors' contributions**

617 Both authors conceived of the approach to the review paper. Both authors contributed to writing this paper.

618 **Acknowledgements**

619 PvK thanks the JpGU for providing travel funding to the most recent pre-COVID and in-person JpGU-AGU meeting
 620 in Chiba, Japan. We thank Geoff Abers, Sambuddha Dhar, and two anonymous reviewers for their comments on and
 621 suggestions for an earlier version of the manuscript. This allowed us to improve the general flow of the manuscript,
 622 the quality of the figures, and in particular the seismological and geodetic descriptions. We also thank Geoff Abers
 623 for providing the heat flow data along the iMUSH profile in Figure 4b.

624 **Endnotes**

625 **References**

- 626 Abers, G.A, van Keken, P.E, Hacker, B.R (2017) The cold and relatively dry nature of mantle forearcs in
 627 subduction zones. *Nat Geosc* 10, 333–337. doi:10.1038/ngeo2922
- 628 Abers, G.A, van Keken, P.E, Kneller, E.A, Ferris, A, Stachnik, J.C (2006) The thermal structure of subduction
 629 zones constrained by seismic imaging: Implications for slab dehydration and wedge flow. *Earth Planet Sci*
 630 *Lett* 241, 387–397. doi:10.1016/j.epsl.2005.11.055
- 631 Abers, G.A, MacKenzie, L.S, Rondenay, S, Zhang, Z, Wech, A.G, Creager, K.C (2009) Imaging the source region
 632 of Cascadia tremor and intermediate-depth earthquakes. *Geology* 37, 1119–1122. doi:10.1130/G30143A.1
- 633 Abers, G.A, Nakajima, J, van Keken, P.E, Kita, S, Hacker, B.R (2013) Thermal-petrological controls on the
 634 location of earthquakes within subducting plates. *Earth Planet Sci Lett* 369–370, 178–187.
 635 doi:10.1016/j.epsl.2013.03.022
- 636 Agata, R, Barbot, S.D, Fujita, K, Hyodo, M, Iinuma, T, Nakata, R, Ichimura, T, Hori, T (2019) Rapid mantle
 637 flow with power-law creep explains deformation after the 2011 Tohoku mega-quake. *Nat Comm* 10. Art No
 638 1385, doi:10.1038/s41467-019-0984-7
- 639 Arzilli, F, Burton, M, La Spina, G, Macpherson, C.G, van Keken, P.E, McCann, J (2023) Decarbonation of
 640 subducting carbonate-bearing sediments and basalts of altered oceanic crust: Insights into recycling of CO₂
 641 through volcanic arcs. *Earth Planet Sci Lett* 602. Art No 117945, doi:10.1016/j.epsl.2022.117945
- 642 Bang, Y, Hwang, H, Kim, T, Cynn, H, Park, Y, Jung, H, Park, C, Popov, D, Prakapenka, V.B, Wang, L,
 643 Liermann, H-P, Irifune, T, Mao, H-K, Lee, Y (2021) The stability of subducted glaucophane with the
 644 Earth's secular cooling. *Nat Comm* 12. Art No 1496, doi:10.1039/s41467-021-21746-8
- 645 Bebout, G.E, Penniston-Dorland, S.C (2016) Fluid and mass transfer at subduction interfaces – The field
 646 metamorphic record. *Lithos* 240–243, 228–258. doi:10.1016/j.lithos.2015.10.007
- 647 Bellot, N, Boyet, M, Doucelance, R, Bonnand, P, Savov, I.P, Plank, T, Elliott, T (2018) Origin of negative cerium
 648 anomalies in subduction-related volcanic samples: Constraints from Ce and Nd isotopes. *Chem Geo* 500,
 649 46–63. doi:10.1016/j.chemgeo.2018.09.006
- 650 Bird, P (2003) An updated digital model of plate boundaries. *Geochem Geophys Geosys* 4. Art No 1027,
 651 doi:10.1029/2001GC000252
- 652 Bloch, W, John, T, Kummerow, J, Salazar, P, Krüger, O, Shapiro, S (2018) Watching dehydration: Seismic
 653 indication for transient fluid pathways in the oceanic mantle of the subducting Nazca slab. *Geochem*
 654 *Geophys Geosys* 19, 3189–3207. doi:10.1029/2018GC007703
- 655 Bostock, M.G (2013) The Moho in subduction zones. *Tectonophysics* 609, 547–557.
 656 doi:10.1016/j.tecto.2012.07.007
- 657 Bostock, M.G, Hyndman, R.D, Rondenay, S, Peacock, S.M (2002) An inverted continental Moho and
 658 serpentinization of the forearc mantle. *Nature* 417, 536–538. doi:10.1038/417536a
- 659 Brey, G.P, Girmis, A.V, Bulatov, V.K, Höfer, H.E, Gerdes, A, Woodland, A.B (2015) Reduced sediment melting at
 660 7.5–12 GPa: phase relations, geochemical signals and diamond nucleation. *Contrib Min Petrol* 170. Art No
 661 18, doi:10.1007/s00410-015-1166-z
- 662 Brocher, T.M, Parsons, T, Tréhu, A, Snelson, C.M, Fisher, M.A (2003) Seismic evidence for widespread
 663 serpentinized forearc upper mantle along the Cascadia margin. *Geology* 31, 267–270.
 664 doi:10.1130/0091-7613(2003)031<0267:SEFWFS>2.0.CO;2
- 665 Brownlee, S.J, Hacker, B.R, Harlow, G.E, Seward, G (2013) Seismic signatures of a hydrated mantle wedge from
 666 antigorite crystal-preferred orientation (CPO). *Earth Planet Sci Lett* 375, 395–407.
 667 doi:10.1016/j.epsl.2013.06.003

- 668 Burdette, E, Hirth, G (2022) Creep rheology of antigorite: Experiments at subduction zone conditions. *J Geophys*
669 *Res: Solid Earth* **127**. Art No e2022JG024260, doi:10.1029/2022JB024260
- 670 Cannàò, E, Tiepolo, M, Bebout, G.E, Scambelluri, M (2020) Into the deep and beyond: Carbon and nitrogen
671 subduction recycling in secondary peridotites. *Earth Planet Sci Lett* **543**. Art No 116328,
672 doi:10.1016/j.epsl.2020.116328
- 673 Cedeño, D.G, Conceição, R.V, Souza, M.R.W, Quinteiro, R.V.C, Carniel, L.C, Ketzer, J.M.M, Rodrigues, F,
674 Bruzza, E.C (2019) An experimental study on smectites as nitrogen conveyors in subduction zones. *Appl*
675 *Clay Sci* **168**, 409–420. doi:10.1016/j.clay.2018.11.006
- 676 Chen, S, Guo, X, Yoshino, T, Jin, Z, Li, P (2018) Dehydration of phengite inferred by electrical conductivity
677 measurements: Implications for the high conductivity anomalies relevant to the subduction zones. *Geology*
678 **46**, 11–14. doi:10.1130/G39716
- 679 Christensen, D.H, Abers, G.A (2010) Seismic anisotropy under central Alaska from SKS splitting observations. *J*
680 *Geophys Res: Solid Earth* **115**. Art No B04315. doi:10.1029/2009JB006712
- 681 Christeson, G.L, Goff, J.A, Reece, R.S (2019) Synthesis of oceanic crustal structure from two-dimensional seismic
682 profiles. *Rev Geophys* **57**, 504–529. doi:10.1029/2019RG000641
- 683 Codillo, E.A, Klein, F, Marschall, H.R (2022) Preferential formation of chlorite over talc during Si-metasomatism
684 of ultramafic rocks in subduction zones. *Geophys Res Lett* **49**. Art No e2022GL100218,
685 doi:10.1029/2022GL100218
- 686 Condit, C.B, Guevara, V.E, Delph, J.R, French, M.E (2020) Slab dehydration in warm subduction zones at depths
687 of episodic slip and tremor. *Earth Planet Sci Lett* **552**. Art No 116601, doi:10.1016/j.epsl.2020.116601
- 688 Crosbie, K.J, Abers, G.A, Mann, M.E, Janiszewski, H.A, Creager, K.C, Ulberg, C.W, Moran, S.C (2019) Shear
689 velocity structure from ambient noise and teleseismic surface wave tomography in the Cascades around
690 Mount St. Helens. *J Geophys Res: Solid Earth* **124**, 8358–8375. doi:10.1029/2019JB017836
- 691 Currie, C.A, Wang, K, Hyndman, R.D, He, J (2004) The thermal effects of steady-state slab-driven mantle flow
692 above a subducting plate: the Cascadia subduction zone and backarc. *Earth Planet Sci Lett* **223**, 35–48.
693 doi:10.1016/j.epsl.2004.04.020
- 694 Dhar, S, Muto, J, Ito, Y, Miura, S, Moore, J.D.P, Ohta, Y, Iinuma, T (2022) Along-arc heterogeneous rheology
695 inferred from post-seismic deformation of the 2011 Tohoku-oki earthquake. *Geophys J Int* **230**, 202–215.
696 doi:10.1093/gji/ggac063
- 697 Dhar, S, Muto, J, Ohta, Y, Iinuma, T (2023) Heterogeneous rheology of Japan subduction zone revealed by
698 postseismic deformation of the 2011 Tohoku-oki earthquake. *Prog Earth Planet Sci* **10**. Art No 9 (2023),
699 doi:10.1186/s40645-023-00539-1
- 700 Eberhart-Phillips, D, Bannister, S, Reyners, M (2020) Attenuation in the mantle wedge beneath super-volcanoes
701 of the Taupo Volcanic Zone, New Zealand. *Geophys J Int* **220**, 703–723. doi:10.1093/gji/ggz455
- 702 Faccenda, M, Gerya, T.V, Mancktelow, N.S, Moresi, L (2012) Fluid flow during slab unbending and dehydration:
703 Implications for intermediate-depth seismicity, slab weakening and deep water recycling. *Geochem Geophys*
704 *Geosys* **13**. Art No Q01010, doi:10.1029/2011GC003860
- 705 Fagereng, Å, Diener, J.F.A, Ellis, S, Remitti, F (2018) Fluid-related deformation processes at the up- and downdip
706 limit of the subduction thrust seismogenic zone: What do the rocks tell us? In: Byrne, T, Underwood III,
707 M.B, Fisher, D, McNeill, L, Saffer, D, Ujiie, K, Yamaguchi, A (eds.) *Geology and Tectonics of Subduction*
708 *Zones: A Tribute to Gaku Kimura*. GSA Special Publication 534. Geological Society of America, Boulder,
709 CO, USA. doi:10.1130/SPE534
- 710 Farsang, S, Louvel, M, Zhao, C, Mezouar, M, Rosa, A.D, Widmer, R.N, Feng, X, Liu, J, Redfern, S.A.T (2021)
711 Deep carbon cycle constrained by carbonate solubility. *Nat Comm* **12**. Art No 4311,
712 doi:10.1038/s41467-021-24533-7
- 713 Faul, U.H, Jackson, I (2005) The seismological signature of temperature and grain size variations in the upper
714 mantle. *Earth Planet Sci Lett* **234**, 119–134. doi:10.1016/j.epsl.2005.02.008
- 715 Ferrand, T.P (2019) Seismicity and mineral destabilizations in the subducting mantle up to 6 GPa, 200 km depth.
716 *Lithos* **334–335**, 205–230. doi:10.1016/j.lithos.2019.03.014
- 717 Fisher, D.M, Smye, A.J, Marone, C, van Keken, P.E, Yamaguchi, A (2019) Kinematic models for healing of the
718 subduction interface based on observations of ancient accretionary complexes. *Geochem Geophys Geosys*
719 **20**, 3431–3449. doi:10.1029/2019GC008256
- 720 Förster, M.W, Selway, K (2021) Melting of subducted sediments reconciles geophysical images of subduction
721 zones. *Nat Comm* **12**. Art No 1320, doi:10.1038/s41467-021-21657-8
- 722 Freed, A.M, Hashima, A, Becker, T.W, Okaya, D, Sato, H, Hatanaka, Y (2017) Resolving depth-dependent
723 subduction zone viscosity and afterslip from postseismic displacements following the 2011 Tohoku-oki,
724 Japan earthquake. *Earth Planet Sci Lett* **456**, 279–290. doi:10.1016/j.epsl.2016.11.040
- 725 Frohlich, C (2006) *Deep Earthquakes*. Cambridge University Press, Cambridge, UK.
726 doi:10.1017/CB09781107297562
- 727 Furukawa, Y (1993) Depth of the decoupling plate interface and thermal structure under arcs. *J Geophys Res:*
728 *Solid Earth* **98**, 20005–20013. doi:10.1029/93JB02020
- 729 Furukawa, Y, Uyeda, S (1989) Thermal state under the Tohoku arc with consideration of crustal heat generation.
730 *Tectonophysics* **164**, 175–187. doi:10.1016/0040-1951(89)90011-5
- 731 Gudmundsson, Ó, Sambridge, M (1998) A regional upper mantle (RUM) seismic model. *J Geophys Res: Solid*
732 *Earth* **103**, 7121–7136. doi:10.1029/97JB02488
- 733 Guo, H, Keppler, H (2019) Electrical conductivity of NaCl-bearing aqueous fluids to 900°C and 5 GPa. *J Geophys*
734 *Res: Solid Earth* **124**, 1397–1411. doi:10.1029/2018JB016658
- 735 Gutscher, M-A, Klingelhoefer, F, Theunissen, T, Spakman, W, Berthet, T, Wang, T.K, Lee, C-S (2016) Thermal
736 modeling of the SW Ryukyu forearc (Taiwan): Implications for the seismogenic zone and the age of the
737 subducting Philippine Sea Plate (Huatung Basin). *Tectonophysics* **692**, 131–142.
738 doi:10.1016/j.tecto.2016.03.029
- 739 Hacker, B.R (2008) H₂O subduction beyond arcs. *Geochem Geophys Geosys* **9**. Art No Q03001,

- doi:10.1029/2007GC001707
- 741 Hacker, B.R, Peacock, S.M, Abers, G.A, Holloway, S.D (2003) Subduction factory 2. Are intermediate-depth
742 earthquakes in subducting slabs linked to metamorphic dehydration reactions? *J Geophys Res: Solid Earth*
743 **108**. Art No 2030, doi:10.1029/2001JB001129
- 744 Hamamoto, H, Yamano, M, Goto, S, Kinoshita, M, Fujino, K, Wang, K (2011) Heat flow distribution and thermal
745 structure of the Nankai subduction zone off the Kii Peninsula. *Geochem Geophys Geosys* **12**. Art No
746 Q0AD20, doi:10.1029/2011GC003623
- 747 Hansen, S.M, Schmandt, B, Levander, A, Kiser, E, Vidale, J.E, Abers, G.A, Creager, K.C (2016) Seismic evidence
748 for a cold serpentinized mantle wedge beneath Mount St Helens. *Nat Comm* **7**. Art No 13242,
749 doi:10.1038/ncoms13242
- 750 Harris, R.N, Grevenmeyer, I, Ranero, C.R, Villinger, H, Backhausen, U, Henke, T, Mueller, C, Neben, S (2010)
751 Thermal regime of the Costa Rican convergent margin: 1. Along-strike variations in heat flow from probe
752 measurements and estimated from bottom-simulating reflectors. *Geochem Geophys Geosys* **11**. Art No
753 Q12S28, doi:10.1029/2010GC003272
- 754 Harris, R, Yamano, M, Kinoshita, M, Spinelli, G, Hadamoto, H, Ashi, J (2013) A synthesis of heat flow
755 determinations and thermal modeling along the Nankai Trough, Japan. *J Geophys Res: Solid Earth* **118**,
756 2687–2702. doi:10.1002/jgrb.50230
- 757 Hayes, G.P, Moore, G.L, Portner, D.E, Flamme, H, Furtney, M, Smoczyk, G.M (2018) Slab 2, a comprehensive
758 subduction zone geometry model. *Science* **362**, 58–61. doi:10.1126/science.aat4723
- 759 Henry, S.G, Pollack, H.N (1988) Terrestrial heat flow above the Andean subduction zone in Bolivia and Peru. *J*
760 *Geophys Res: Solid Earth* **93**, 15153–15162. doi:10.1029/JB093iB12p15153
- 761 Henrys, S.A, Ellis, S, Uruski, C (2003) Conductive heat flow variations from bottom-simulating reflectors on the
762 Hikurangi margin, New Zealand. *Geophys Res Lett* **30**. Art No 1065, doi:10.1029/2002GL015772
- 763 Hermann, J, Lakey, S (2021) Water transfer to the deep mantle through hydrous, Al-rich silicates in subduction
764 zones. *Geology* **49**, 911–915. doi:10.1130/G48658.1
- 765 Hernández-Urbe, D, Hernández-Montenegro, J.D, Cone, K.A, Palin, R.M (2019) Oceanic slab-top melting during
766 subduction: Implications for trace-element recycling and adakite petrogenesis. *Geology* **48**, 216–220.
767 doi:10.1130/G46835.1
- 768 Hicks, S.P, Bie, L, Rychert, C.A, Harmon, N, Goes, S, Rietbrock, A, Wei, S.S, Collier, J, Henstock, T.J, Lynch, L,
769 Prytulak, J, MacPherson, C.G, Schlaphorst, D, Wilkinson, J.J, Blundy, J.D, Cooper, G.F, Davey, R.G,
770 Kendall, J-M, VoiLA Working Group (2023) Slab to back-arc to arc: Fluid and melt pathways through the
771 mantle wedge beneath the Lesser Antilles. *Sci Adv* **9**. Art No eadd2143, doi:10.1126/sciadv.add2143
- 772 Hirauchi, K-i, Katayama, I, Kouketsu, Y (2020) Semi-brittle deformation of antigorite serpentinite under forearc
773 mantle wedge conditions. *J Struct Geol* **140**. Art No 104151, doi:10.1016/j.jsg.2020.104151
- 774 Honda, S (1985) Thermal structure beneath Tohoku, northeast Japan – a case study for understanding the
775 detailed thermal structure of the subduction zone. *Tectonophysics* **112**, 69–102.
776 doi:10.1016/0040-1951(85)90173-8
- 777 Horiuchi, S-s, Iwamori, H (2016) A consistent model for fluid distribution, viscosity distribution, and flow-thermal
778 structure in subduction zone. *J Geophys Res: Solid Earth* **121**, 3238–3260. doi:10.1002/2015JB012384
- 779 Horn, C, Bouilhol, P, Skemer, P (2020) Serpentinization, deformation, and seismic anisotropy in the subduction
780 mantle wedge. *Geochem Geophys Geosys* **21**. Art No e2020GC008950, doi:10.1029/2020GC008950
- 781 Hu, H, Dai, L, Li, H, Hui, K, Sun, W (2017) Influence of dehydration on the electrical conductivity of epidote and
782 implications for high-conductivity anomalies in subduction zones. *J Geophys Res: Solid Earth* **122**,
783 2751–2762. doi:10.1002/2016JB013767
- 784 Hu, Y, Teng, F-Z, Chauvel, C (2021) Potassium isotopic evidence for sedimentary input to the mantle source of
785 Lesser Antilles lavas. *Geochim Cosmochim Acta* **295**, 91–111. doi:10.1016/j.gca.2020.12.013
- 786 Hu, Y, Teng, F-Z, Ionov, D.A (2020) Magnesium isotopic composition of metasomatized upper sub-arc mantle
787 and its implications to Mg cycling in subduction zones. *Geochim Cosmochim Acta* **278**, 219–234.
788 doi:10.1016/j.gca.2019.09.030
- 789 Hu, Y, Bürgmann, R, Uchida, N, Banerjee, P, Freymueller, J.T (2014) Stress-driven relaxation of heterogeneous
790 upper mantle and time-dependent afterslip following the 2011 Tohoku earthquake. *J Geophys Res: Solid*
791 *Earth* **121**, 385–411. doi:10.1002/2015JB012508
- 792 Huang, Y, Guo, H, Nakatani, T, Uesugi, K, Nakamura, M, Keppler, H (2021) Electrical conductivity in texturally
793 equilibrated fluid-bearing forsterite aggregates at 800°C and 1 GPa: Implications for the high electrical
794 conductivity anomalies in mantle wedges. *J Geophys Res: Solid Earth* **126**. Art No e2020JB021343,
795 doi:10.1029/2020JB021343
- 796 Hyndman, R.D, Davis, E.E, Wright, J.A (1979) The measurement of marine geothermal heat flow by a
797 multipenetration probe with digital acoustic telemetry and insitu thermal conductivity. *Mar Geophys Res* **4**,
798 181–205. doi:10.1007/BF00286404
- 799 Hyndman, R.D, Wang, K, Yamano, M (1995) Thermal constraints on the seismogenic portion of southwestern
800 Japan subduction thrust. *J Geophys Res: Solid Earth* **100**, 15373–15392. doi:10.1029/95JB00153
- 801 Hyndman, R.D, Foucher, J.P, Yamano, M, Fisher, A, Scientific Team of Ocean Drilling Program Leg 131 (1992)
802 Deep sea bottom-simulating reflectors: calibration of the base of the hydrate stability field as used for heat
803 flow estimates. *Earth Planet Sci Lett* **109**, 289–301. doi:10.1016/0012-821X(92)90093-B
- 804 Jang, H, Kim, Y.H, Lim, H, Clayton, R.W (2019) Seismic attenuation structure of southern Peruvian subduction
805 system. *Tectonophysics* **771**. Art No 228203, doi:10.1016/j.tecto.2019.228203
- 806 Jégo, S, Dasgupta, J (2013) Fluid-present melting of sulfide-bearing ocean-crust: Experimental constraints on the
807 transport of sulfur from subducting slab to mantle wedge. *Geochim Cosmochim Acta* **110**, 106–134.
808 doi:10.1016/j.gca.2013.02.011
- 809 Jégo, S, Dasgupta, J (2014) The fate of sulfur during fluid-present melting of subducting basaltic crust at variable
810 oxygen fugacity. *J Petrol* **55**, 1019–1050. doi:10.1093/petrology/egu016
- 811 Ji, Y, Yoshioka, S, Matsumoto, T (2016) Three-dimensional numerical modeling of temperature and mantle flow

- 812 fields associated with subduction of the Philippine Sea plate, southwest Japan. *J Geophys Res: Solid Earth*
813 121, 4458–4482. doi:10.1002/2016JB012912
- 814 Jung, H, Green II, H.W, Dobrzhinetskaya, L.F (2004) Intermediate-depth earthquake faulting by dehydration
815 embrittlement with negative volume change. *Nature* 428, 545–549. doi:10.1038/nature02412
- 816 Katayama, I, Hirauchi, K-i, Michibayashi, K, Ando, J-i (2009) Trench-parallel anisotropy produced by serpentinite
817 deformation in the hydrated mantle wedge. *Nature* 461, 1114–1117. doi:10.1038/nature08513
- 818 Kelemen, P.B, Hirth, G (2007) A periodic shear-heating mechanism for intermediate-depth earthquakes in the
819 mantle. *Nature* 446, 787–790. doi:10.1038/nature05717
- 820 Kerswell, B.C, Kohn, M.J, Gerya, T.V (2021) Backarc lithospheric thickness and serpentine stability control
821 slab-mantle coupling depths in subduction zones. *Geochem Geophys Geosys* 22. Art No e2022GC009304,
822 doi:10.1029/2020GC009304
- 823 Kim, H.J, Kawakatsu, H, Akuhara, T, Shinohara, M, Shiobara, H, Sugioka, H, Takagi, R (2021) Receiver function
824 imaging of the amphibious NE Japan subduction zone – Effects of low-velocity sediment layer. *J Geophys*
825 *Res: Solid Earth* 126. Art No e2021JB021918, doi:10.1029/2021JB021918
- 826 Kimura, J-I (2017) Modeling chemical geodynamics of subduction zones using the Arc Basalt Simulator version 5.
827 *Geosphere* 13, 992–1025. doi:10.1130/GES01468.1
- 828 Kimura, J-I, Nakajima, J (2014) Behaviour of subducted water and its role in magma genesis in the NE Japan arc:
829 A combined geophysical and geochemical approach. *Geochim Cosmochim Acta* 143, 165–188.
830 doi:10.1016/j.gca.2014.04.019
- 831 Kimura, J-I, Stern, R.J, Yoshida, T (2005) Reinitiation of subduction and magmatic responses in SW Japan
832 during Neogene time. *GSA Bull* 117, 969–986. doi:10.1130/B25565.1
- 833 Kimura, J-I, Hacker, B.R, van Keken, P.E, Kawabata, H, Yoshida, T, Stern, R.J (2009) Arc Basalt Simulator
834 version 2, a simulation for slab dehydration and fluid-flux mantle melting for arc basalts: Modeling scheme
835 and application. *Geochem Geophys Geosys* 10. Art No Q09004, doi:10.1029/2008GC002217
- 836 Kimura, J-I, Kent, A.J.R, Rowe, M, Katakuse, M, Nakano, F, Hacker, B.R, van Keken, P.E, Kawabata, H, Stern,
837 R.J (2010) Origin of cross-chain geochemical variation in Quaternary lavas from the northern Izu arc: Using
838 a quantitative mass balance approach to identify mantle sources and wedge processes. *Geochem Geophys*
839 *Geosys* 11. Art No Q10011, doi:10.1029/2010GC003050
- 840 Kimura, J-I, Gill, J.B, Kunikiyo, T, Osaka, I, Shimoshiori, Y, Katakuse, M, Kakabuchi, S, Nagao, T, Furuyama, K,
841 Kamei, A, Kawabata, H, Nakajima, J, van Keken, P.E, Stern, R.J (2014) Diverse magmatic effects of
842 subducting a hot slab in SW Japan: Results from forward modeling. *Geochem Geophys Geosys* 15, 691–739.
843 doi:10.1002/2013GC005132
- 844 Kimura, J-I, Gill, J.B, Skora, S, van Keken, P.E, Kawabata, H (2016) Origin of geochemical mantle components:
845 Role of subduction filter. *Geochem Geophys Geosys* 17, 3289–3325. doi:10.1002/2016GC006343
- 846 Kirby, S, Engdahl, E.R, Denlinger, R (1996) Intermediate-depth intraslab earthquakes and arc volcanism as
847 physical expressions of crustal and uppermost mantle metamorphism in subducting slabs. In: *Bebout, G.E,*
848 *Scholl, D.W, Kirby, S.H, Platt, J.P (eds.) Subduction: Top to Bottom, Geophysical Monograph* 96.
849 *American Geophysical Union, Washington, DC, USA*, pp 195–214. doi:10.1029/GM096
- 850 Kita, S, Okada, T, Hasegawa, A, Nakajima, J, Matsuzawa, T (2010a) Anomalous deepening of a seismic belt in
851 the upper-plane of the double seismic zone in the Pacific slab beneath the Hokkaido corner: Possible
852 evidence for thermal shielding caused by subducted forearc crust materials. *Earth Planet Sci Lett* 290,
853 415–426. doi:10.1016/j.epsl.2009.12.038
- 854 Kita, S, Okada, T, Hasegawa, A, Nakajima, J, Matsuzawa (2010b) Existence of interplane earthquakes and
855 neutral stress boundary between the upper and lower planes of the double seismic zone beneath Tohoku and
856 Hokkaido, northeastern Japan. *Tectonophysics* 496, 68–82. doi:10.1016/j.tecto.2010.10.010
- 857 Kneller, E.A, Long, M.D, van Keken, P.E (2008) Olivine fabric transitions and shear wave anisotropy in the
858 Ryukyu subduction system. *Earth Planet Sci Lett* 268, 268–282. doi:10.1016/j.epsl.2008.01.004
- 859 Kneller, E.A, van Keken, P.E, Katayama, I, Karato, S (2007) Stress, strain, and B-type olivine fabric in the
860 fore-arc mantle: Sensitivity tests using high-resolution steady-state subduction zone models. *J Geophys Res:*
861 *Solid Earth* 222. Art No B04406, doi:10.1029/2006JB004544
- 862 Ko, Y-T, Kuo, B-Y, Wang, K-L, Lin, S-C, Hung, S-H (2012) The southwestern edge of the Ryukyu subduction
863 zone: A high Q mantle wedge. *Earth Planet Sci Lett* 335–336, 145–153. doi:10.1016/j.epsl.2012.04.041
- 864 Lee, J, Mookherjee, M, Kim, T, Jung, H, Klemd, R (2021) Seismic anisotropy in subduction zones: Evaluating the
865 role of chloritoid. *Front Earth Sci* 9. Art No 644958, doi:10.3389/feart.2021.644958
- 866 Long, M.D, van der Hilst, R.D (2005) Upper mantle anisotropy beneath Japan from shear wave splitting. *Phys*
867 *Earth Planet Inter* 151, 206–222. doi:10.1016/j.pepi.2005.03.003
- 868 Long, M.D, van der Hilst, R.D (2006) Shear wave splitting from local events beneath the Ryukyu arc:
869 Trench-parallel anisotropy in the mantle wedge. *Phys Earth Planet Inter* 155, 300–312.
870 doi:10.1016/j.pepi.2006.01.003
- 871 Loveless, J.P, Meade, B.J (2011) Spatial correlation of interseismic coupling and coseismic rupture extent of the
872 2011 $M_w=9.0$ Tohoku-oki earthquake. *Geophys Res Lett* 38. Art No L17306, doi:10.1029/2011GL048561
- 873 Luo, H, Wang, K (2021) Postseismic geodetic signature of cold forearc mantle in subduction zones. *Nat Geosc* 14,
874 104–109. doi:10.1038/s41561-020-00679-9
- 875 Manea, M, Manea, V.C (2011) Curie point depth estimates and correlation with subduction in Mexico. *Pure Appl*
876 *Geophys* 168, 1489–1499. doi:10.1007/s00024-010-0238-2
- 877 Mann, M.E, Abers, G.A, Crosbie, K, Creager, K, Ulberg, C, Moran, S, Rondenay, S (2019) Imaging subduction
878 beneath Mount St. Helens: Implications for slab dehydration and magma transport. *Geophys Res Lett* 46,
879 3163–3171. doi:10.1029/2018GL081471
- 880 Manthilake, G, Koga, K.T, Peng, Y, Mookherjee, M (2021) Halogen bearing amphiboles, aqueous fluids, and
881 melts in subduction zones: Insights on halogen cycle from electrical conductivity. *J Geophys Res: Solid Earth*
882 126. Art No e2020JB021339, doi:10.1029/2020JB021339
- 883 Marcaillou, B, Spence, G, Wang, K, Collet, J-Y, Ribodetti, A (2008) Thermal segmentation along the

- 884 N. Ecuador–S. Columbia margin (1–4°N): Prominent influence of sedimentation rate in the trench. *Earth*
 885 *Planet Sci Lett* 272, 296–308. doi:10.1016/j.epsl.2008.04.049
- 886 Marschall, H.R., Schumacher, J.C. (2012) Arc magmas sourced from mélange diapirs in subduction zones. *Nat*
 887 *Geosc* 5, 862–867. doi:10.138/ngeo1634
- 888 Martindale, M., Skora, S., Pickles, J., Elliott, T., Blundy, J., Avanzinelli, R. (2013) High pressure phase relations of
 889 subducted volcanoclastic sediments from the west Pacific and their implications for the geochemistry of
 890 Mariana arc magmas. *Chem Geo* 342, 94–109
- 891 Mazza, S.E., Stracke, A., Gill, J.B., Kimura, J.-I., Kleine, T. (2020) Tracing dehydration and melting of the subducted
 892 slab with tungsten isotopes in arc lavas. *Earth Planet Sci Lett* 530. Art No 115942,
 893 doi:10.1016/j.epsl.2019.115942
- 894 McCormack, K., Wirth, E.A., Long, M.D. (2013) B-type olivine fabric and mantle wedge serpentinization beneath
 895 the Ryukyu arc. *Geophys Res Lett* 40, 1697–1702. doi:10.1002/grl.50369
- 896 Merkulova, M., Muñoz, M., Vidal, O., Brunet, F. (2016) Role of iron content on serpentinite dehydration depth in
 897 subduction zones: Experiments and thermodynamic modeling. *Lithos* 264, 441–452.
 898 doi:10.1016/j.lithos.2016.09.007
- 899 Molnar, P., England, P. (1990) Temperature, heat flux, and frictional stress near major thrust faults. *J Geophys*
 900 *Res: Solid Earth* 95, 4833–4856. doi:10.1029/JB095iB04p04833
- 901 Mookherjee, M., Capitani, G.C. (2011) Trench parallel anisotropy and large delay times: Elasticity and anisotropy of
 902 antigorite at higher pressures. *Geophys Res Lett* 38. Art No L09315, doi:10.1029/2011GL047160
- 903 Morishige, M. (2022) The thermal structure of subduction zones predicted by plate cooling models with variable
 904 thermal properties. *Geophys J Int* 229, 1490–1502. doi:10.1093/gji/ggac008
- 905 Morishige, M., Honda, S. (2013) Mantle flow and deformation of subducting slab at a plate junction. *Earth Planet*
 906 *Sci Lett* 365, 132–142. doi:10.1016/j.epsl.2013.01.033
- 907 Morishige, M., van Keken, P.E. (2014) Along-arc variation in the 3-D thermal structure around the junction
 908 between the Japan and Kurile arcs. *Geochem Geophys Geosys* 15, 2225–2240. doi:10.1002/2014GC005394
- 909 Morishige, M., van Keken, P.E. (2017) Along-arc variation in short-term slow slip events caused by 3-D fluid
 910 migration in subduction zones. *J Geophys Res: Solid Earth* 122, 1434–1448. doi:10.1002/2016JB013091
- 911 Müller, R.D., Sdrolias, M., Gaina, C., Roest, R.W. (2008) Age, spreading rates, and spreading asymmetry of the
 912 world's ocean crust. *Geochem Geophys Geosys* 9. Art No Q04006, doi:10.1029/2007GC001743
- 913 Muto, J., Shibazaki, B., Iinuma, T., Ito, Y., Ohta, Y., Miura, S., Nakai, Y. (2016) Heterogeneous rheology controlled
 914 postseismic deformation of the 2011 Tohoku-Oki earthquake. *Geophys Res Lett* 43, 4971–4978.
 915 doi:10.1002/2016GL068113
- 916 Muto, J., Moore, J.D.P., Barbot, S., Iinuma, T., Ohta, Y., Iwamori, H. (2019) Coupled afterslip and transient flow
 917 after the 2011 Tohoku earthquake. *Sci Adv* 5. Art No eaaw1164, doi:10.1126/sciadv.aaw1164
- 918 Nagaya, T., Walker, A.M., Wookey, J., Wallis, S.R., Ishii, K., Kendall, J.-M. (2016) Seismic evidence for flow in the
 919 hydrated mantle wedge of the Ryukyu subduction zone. *Sci Rep* 6. Art No 29981, doi:10.1038/srep29981
- 920 Nakajima, J., Hasegawa, A. (2004) Shear-wave polarization anisotropy and subduction-induced flow in the mantle
 921 wedge of northeastern Japan. *Earth Planet Sci Lett* 225, 365–377. doi:10.1016/j.epsl.2004.06.011
- 922 Nakajima, J., Hada, S., Hayami, E., Uchida, N., Hasegaswa, A., Yoshioka, S., Matsuzawa, T., Umino, N. (2013)
 923 Seismic attenuation beneath northeastern Japan: Constraints on mantle dynamics and arc magmatism. *J*
 924 *Geophys Res: Solid Earth* 118, 5838–5855. doi:10.1002/2013JB010388
- 925 Ohde, A., Otsuka, H., Kioka, A., Ashi, J. (2018) Distribution and depth of bottom-simulating reflectors in the
 926 Nankai subduction zone. *Earth Planets Space* 70. Art No 60, doi:10.1186/s40623-018-0833-5
- 927 Okubo, Y., Matsunaga, T. (1994) Curie point depth in northeast Japan and its correlation with regional thermal
 928 structure and seismicity. *J Geophys Res: Solid Earth* 99, 22363–22371. doi:10.1029/94JB01336
- 929 Padrón-Navarta, J.A., Tommasi, A., Garrido, C.J., Sánchez-Vizcaíno, V.L., Gómez-Pugnaire, M.T., Jabaloy, A.,
 930 Vauchez, A. (2010) Fluid transfer into the mantle wedge controlled by high-pressure hydrofracturing in the
 931 cold top-slab mantle. *Earth Planet Sci Lett* 297, 271–286. doi:10.1016/j.epsl.2010.06.029
- 932 Pang, G., Abers, G.A., van Keken, P.E. (2023) Focusing effects of teleseismic wavefields by the subducting plate
 933 beneath Cascadia. *J Geophys Res: Solid Earth* 128. Art No e2022JB025486, doi:10.1029/2022JB025486
- 934 Peacock, S.M. (2001) Are the lower planes of double seismic zones caused by serpentine dehydration in subducting
 935 oceanic mantle? *Geology* 29, 299–302. doi:10.1130/0091-7613(2001)029<0299:ATLPOD>2.0.C
- 936 Peacock, S.M. (2020) Advances in the thermal and petrologic modeling of subduction zones. *Geosphere* 16,
 937 936–952. doi:10.1130/GES02213.1
- 938 Peacock, S.M., Wang, K. (2021) On the stability of talc in subduction zones: A possible control on the maximum
 939 depth of decoupling between subducting plate and mantle wedge. *Geophys Res Lett* 48. Art No
 940 e2021GL094889, doi:10.1029/2021GL094889
- 941 Peña, C., Heidback, O., Moreno, M., Bedford, J., Ziegler, M., Tassara, A., Oncken, O. (2020) Impact of power-law
 942 rheology on the viscoelastic relaxation pattern and afterslip distribution following the 2010 Mw 8.8 Maule
 943 earthquake. *Earth Planet Sci Lett* 542. Art No 116292, doi:10.1016/j.epsl.2020.116292
- 944 Piccoli, F., Vitale Brovarone, A., Beyssac, O., Martinez, I., Ague, J.J., Chaduteau, C. (2016) Carbonation by
 945 fluid-rock interactions at high-pressure conditions: Implications for carbon cycling in subduction zones.
 946 *Earth Planet Sci Lett* 445, 146–158. doi:10.1016/j.epsl.2016.03.045
- 947 Pollack, H.N., Hurter, S.J., Johnson, J.R. (1993) Heat flow from Earth's interior: Analysis of the global data set.
 948 *Rev Geophys* 31, 267–280. doi:10.1029/93RG01249
- 949 Pommier, A., Evans, R.L. (2017) Constraints on fluids in subduction zones from electromagnetic data. *Geosphere*
 950 13, 1026–1041. doi:10.1130/GES01473.1
- 951 Pommier, A., Williams, Q., Evans, R.L., Pal, I., Zhang, Z. (2019) Electrical investigations of natural lawsonite and
 952 application to subduction contexts. *J Geophys Res: Solid Earth* 124, 1430–1442.
 953 doi:10.1029/2018JB016899
- 954 Portner, D.E., Hayes, G.P. (2018) Incorporating teleseismic tomography data into models of upper mantle slab
 955 geometry. *Geophys J Int* 215, 325–332. doi:10.1093/gji/ggy279

- 956 Pozgay, S.H, Wiens, D.A, Conder, J.A, Shiobara, H, Sugioka, H (2009) Seismic attenuation tomography of the
 957 Mariana subduction system: Implications for thermal structure, volatile distribution, and slow spreading
 958 dynamics. *Geochem Geophys Geosys* **10**. Art No Q04X05, doi:10.1029/2008GC002313
- 959 Prakash, A, Holyoke III, C.W, Kelemen, P.B, Kirby, S.H, Kronenberg, A.K, Lamb, W.M (2023) Carbonates and
 960 intermediate-depth seismicity: Stable and unstable shear in altered subducting plates and overlying mantle.
 961 *Proc Nat Acad Sci* **120**. Art No e2219076120, doi:10.1073/pnas.2219076120
- 962 Raleigh, C.B, Paterson, M.S (1965) Experimental deformation of serpentinite and its tectonic implications. *J*
 963 *Geophys Res: Solid Earth* **70**, 3965–3985. doi:10.1029/JZ070i016p03965
- 964 Reynard, B (2013) Serpentine in active subduction zones. *Lithos* **178**, 171–185. doi:10.1016/j.lithos.2012.10.012
- 965 Rogers, G, Dragert, H (2003) Episodic tremor and slip on the Cascadia subduction zone: The chatter of silent slip.
 966 *Science* **300**, 1942–1943. doi:10.1126/science.1084783
- 967 Rondenay, S, Abers, G.A, van Keken, P.E (2008) Seismic imaging of subduction zone metamorphism. *Geology* **36**,
 968 275–278. doi:10.1130/G24112A.1
- 969 Rüpke, L.H, Phipps Morgan, J, Hort, M, Connolly, J.A.D (2004) Serpentine and the subduction zone water cycle.
 970 *Earth Planet Sci Lett* **223**, 17–34. doi:10.1016/j.epsl.2004.04.018
- 971 Rustioni, G, Audetat, A, Keppler, H (2021) The composition of subduction zone fluids and the origin of the trace
 972 element enrichment in arc magmas. *Contrib Min Petrol* **176**. Art No 51, doi:10.1007/s00410-021-01810-8
- 973 Rychert, C.A, Fischer, K.M, Abers, G.A, Plank, T, Syracuse, E, Protti, J.M, Gonzalez, V, Strauch, W (2008)
 974 Strong along-arc variations in attenuation in the mantle wedge beneath Costa Rica and Nicaragua.
 975 *Geochem Geophys Geosys* **9**. Art No Q10S10, doi:10.1029/2008GC002040
- 976 Sacks, I.S (1968) Distribution of absorption of shear waves in South America and its tectonic significance.
 977 *Carnegie Inst Year Book* **67**, 339–344. <https://archive.org/details/yearbookcarne67196768carn>
- 978 Saita, H, Nakajima, J, Shiina, T, Kimura, J-I (2015) Slab-derived fluids, fore-arc hydration, and sub-arc
 979 magmatism beneath Kyushu, Japan. *Geophys Res Lett* **42**, 1685–1693. doi:10.1012/2015GL063084
- 980 Salmi, M.S, Johnson, P.J, Harris, R.N (2017) Thermal environment of the Southern Washington region of the
 981 Cascadia subduction zone. *J Geophys Res: Solid Earth* **122**, 5852–5870. doi:10.1002/2016JB013839
- 982 Seno, T (1977) The instantaneous rotation vector of the Philippine sea plate relative to the Eurasian plate.
 983 *Tectonophysics* **42**, 209–226. doi:10.1016/0040-1951(77)90168-8
- 984 Seno, T, Maruyama, S (1984) Paleogeographic reconstruction and origin of the Philippine Sea. *Tectonophysics*
 985 **102**, 53–84. doi:10.1016/0040-1951(84)90008-8
- 986 Shelly, D.R, Beroza, G.C, Ide, S, Nakamura, S (2006) Low-frequency earthquakes in Shikoku, Japan, and their
 987 relationship to episodic tremor and slip. *Nature* **442**, 188–191. doi:10.1038/nature04931
- 988 Shiina, T, Nakajima, J, Matsuzawa, T (2013) Seismic evidence for high pore pressures in oceanic crust:
 989 Implications for fluid-related embrittlement. *Geophys Res Lett* **40**, 2006–2010. doi:10.1002/grl.50468
- 990 Shiina, T, Nakajima, J, Matsuzawa, T, Toyokuni, G, Kita, S (2017) Depth variations in seismic velocity in the
 991 subducting crust: Evidence for fluid-related embrittlement for intermediate-depth earthquakes. *Geophys Res*
 992 *Lett* **44**, 810–817. doi:10.1002/2016GL071798
- 993 Shimoda, G, Kogiso, T (2019) Effect of serpentinite dehydration in subducting slab on isotopic diversity in
 994 recycled oceanic crust and its role in isotopic heterogeneity of the mantle. *Geochem Geophys Geosys* **20**,
 995 5449–5472. doi:10.1029/2019GC008336
- 996 Shirey, S.B, Wagner, L.S, Walter, M.J, Pearson, D.G, van Keken, P.E (2021) Slab transport of fluids to deep
 997 focus earthquake depths – thermal modeling constraints and evidence from diamonds. *AGU Advances* **2**. Art
 998 No e2020AV000304, doi:10.1029/2020AV000304
- 999 Sippl, C, Schurr, B, John, T, Hainzl, S (2019) Filling the gap in a double seismic zone: Intraslab seismicity in
 1000 northern Chile. *Lithos* **346–347**. Art No 105155, doi:10.1016/j.lithos.2019.105155
- 1001 Smye, A.J, Jackson, C.R.M, Konrad-Schmolke, M, Hesse, M.A, Parman, S.W, Shuster, D.L, Ballentine, C.J
 1002 (2017) Noble gases recycled into the mantle through cold subduction zones. *Earth Planet Sci Lett* **471**,
 1003 65–73. doi:10.1016/j.epsl.2017.04.046
- 1004 Springer, M, Förster, A (1998) Heat-flow density across the Central Andean subduction zone. *Tectonophysics* **291**,
 1005 123–139. doi:10.1016/S0040-1951(98)00035-3
- 1006 Stachnik, J.C, Abers, G.A, Christensen, G.A (2004) Seismic attenuation and mantle wedge temperatures in the
 1007 Alaska subduction zone. *J Geophys Res: Solid Earth* **109**. Art No B10304, doi:10.1029/2004JGB003018
- 1008 Suenaga, N, Yoshioka, S, Ji, Y (2021) 3-D thermal regime and dehydration processes around the regions of slow
 1009 earthquakes along the Ryukyu Trench. *Sci Rep* **11**. Art No 11251, doi:10.1038/s41598-021-90199-2
- 1010 Suenaga, N, Yoshioka, S, Matsumoto, T, Ji, Y (2018) Two-dimensional thermal modeling associated with the
 1011 subduction of the Philippine Sea plate in southern Kyushu, Japan. *Tectonophysics* **723**, 288–296.
 1012 doi:10.1016/j.tecto.2017.12.017
- 1013 Suenaga, N, Yoshioka, S, Matsumoto, T, C, M.V, Manea, M, Ji, Y (2019) Two-dimensional thermal modeling of
 1014 the Philippine Sea plate subduction in central Japan: Implications for gap of low-frequency earthquakes and
 1015 tectonic tremors. *J Geophys Res: Solid Earth* **124**, 6848–6865. doi:10.1029/2018JB017068
- 1016 Syracuse, E.M, Abers, G.A (2006) Global compilation of variations in slab depth beneath arc volcanoes and
 1017 implications. *Geochem Geophys Geosys* **7**. Art No Q05107, doi:10.1029/2005GC001045
- 1018 Syracuse, E.M, van Keken, P.E, Abers, G.A (2010) The global range of subduction zone thermal models. *Phys*
 1019 *Earth Planet Int* **183**, 73–90. doi:10.1016/j.pepi.2010.02.004
- 1020 Takei, Y (2017) Effects of partial melting on seismic velocity and attenuation: A new insight from experiments.
 1021 *Ann Rev Earth Planet Sci* **45**, 447–470. doi:10.1146/annurev-earth-063016-015820
- 1022 Tanaka, A, Yamano, Y, Yano, Y, Sasada, M (2004) Geothermal gradient and heat flow data in and around Japan
 1023 (I): Appraisal of heat flow from geothermal gradient data. *Earth Planets Space* **56**, 1191–1194.
 1024 doi:10.1186/BF03353339
- 1025 Tian, M, Katz, R.F, Rees Jones, D.W, May, D.A (2019) Devolatilization of subduction slabs, part II: Volatile
 1026 fluxes and storage. *Geochem Geophys Geosys* **20**, 6199–6222. doi:10.1029/2019GC008489
- 1027 Tsuno, K, Dasgupta, R, Danielson, L, Righter, K (2012) Flux of carbonate melt from deeply subducted pelitic

- sediments: Geophysical and geochemical implications for the source of Central American volcanic arc. *Geophys Res Lett* **39**. Art No L16307, doi:10.1029/2012GL052606
- Uchide, N, Nakajima, J, Wang, K, Takagi, R, Yoshida, K, Nakayama, T, Hino, R, Okada, T, Asano, Y (2020) Stagnant forearc mantle wedge inferred from mapping of shear-wave anisotropy using S-net seafloor seismometers. *Nat Comm* **11**. Art No 5676, doi:10.1038/s41467-020-19541-y
- Utsu, T (1966) Regional differences in absorption of seismic waves in the upper mantle as inferred from abnormal distributions of seismic intensities. *Journal of the Faculty of Science, Hokkaido University, ser. VII*, **2**, 359–374
- van Dinther, Y, Preiswerk, L.E, Gerya, T.V (2019) A secondary zone of uplift due to megathrust earthquakes. *Pure Appl Geophys* **176**, 4043–4068. doi:10.1007/s00024-019-02250-z
- van Keken, P.E (2003) The structure and dynamics of the mantle wedge. *Earth Planet Sci Lett* **215**, 323–338. doi:10.1016/S0012-821X(03)00460-6
- van Keken, P.E, Kiefer, B, Peacock, S.M (2002) High-resolution models of subduction zones: Implications for mineral dehydration reactions and the transport of water to the deep mantle. *Geochem Geophys Geosys* **3**. Art No 1056, doi:10.1029/2001GC000256
- van Keken, P.E, Kita, S, Nakajima, J (2012) Thermal structure and intermediate-depth seismicity in the Tohoku-Hokkaido subduction zones. *Solid Earth* **3**, 355–364. doi:10.5194/se-3-355-2012
- van Keken, P.E, Hacker, B.R, Syracuse, E.M, Abers, G.A (2011) Subduction factory: 4. Depth-dependent flux of H₂O from subducting slabs worldwide. *J Geophys Res: Solid Earth* **116**. Art No B01401, doi:10.1029/2010JB007922
- van Keken, P.E, Wada, I, Sime, N, Abers, G.A (2019) Thermal structure of the forearc in subduction zones: A comparison of methodologies. *Geochem Geophys Geosys* **20**, 3268–3288. doi:10.1029/2019GC008334
- Ventouzi, C, Papazachos, C, Hatzidimitriou, P, Papaioannou, C, EGALADOS Working Group (2018) Anelastic P- and S- upper mantle attenuation tomography of the southern Aegean Sea subduction area (Hellenic Arc) using intermediate-depth earthquake data. *Geophys J Int* **215**, 635–658. doi:10.1093/gji/ggy292
- Vho, A, Lanari, P, Rubatto, D, Hermann, J (2020) Tracing fluid transfers in subduction zones: an integrated thermodynamic and $\delta^{18}\text{O}$ fractionation modelling approach. *Solid Earth* **11**, 307–328. doi:10.5194/se-11-307-2020
- Vitale Brovarone, A, Beyssac, O (2014) Lawsonite metasomatism: A new route for water to the deep Earth. *Earth Planet Sci Lett* **393**, 275–284. doi:10.1016/j.epsl.2014.03.001
- Von Herzen, R, Ruppel, C, Molnar, P, Nettles, M, Nagihara, S, Ekström, G (2001) A constraint on the shear stress at the Pacific-Australian plate boundary from heat flow and seismicity at the Kermadec forearc. *J Geophys Res: Solid Earth* **106**, 6817–6833. doi:10.1029/2000JB900469
- Wada, I, He, J (2017) Thermal structure of the Kanto region, Japan **44**, 7194–7202. doi:10.1002/2017GL073597
- Wada, I, King, S.D (2015) Dynamics of subducting slabs: Numerical modeling and constraints from seismology, geoid, topography, geochemistry, and petrology. In: Schubert, G (ed.) *Treatise on Geophysics* (2nd Edition), Volume 7 "Mantle Dynamics" (Bercovici, D (ed.)) pp 339–391. Elsevier, Amsterdam, The Netherlands. doi:10.1016/B978-0-444-53802-4.00132-9
- Wada, I, Wang, K (2009) Common depth of slab-mantle decoupling: Reconciling diversity and uniformity of subduction zones. *Geochem Geophys Geosys* **10**. Art No Q10009, doi:10.1029/2009GC002570
- Wada, I, Wang, K, He, J, Hyndman, R.D (2008) Weakening of the subduction interface and its effects on surface heat flow, slab dehydration, and mantle wedge serpentinization. *J Geophys Res: Solid Earth* **113**. Art No B04402, doi:10.1029/2007JB005190
- Wada, I, He, J, Hasegawa, A, Nakajima, J (2015) Mantle wedge flow patterns and thermal structure in Northeast Japan: Effects of oblique subduction and 3-D slab geometry. *Earth Planet Sci Lett* **426**, 76–88. doi:10.1006/j.epsl.2015.06.021
- Wang, J, Huang, X, Zhao, D, Yao, Z (2019) Seismic anisotropy evidence for ductile deformation of the forearc lithospheric mantle in subduction zones. *J Geophys Res: Solid Earth* **124**, 7013–7027. doi:10.1029/2018JB016912
- Wang, K, Wada, I, Ishikawa, Y (2004) Stresses in the subducting slab beneath southwest Japan and relation with plate geometry, tectonic forces, slab dehydration, and damaging earthquakes. *J Geophys Res: Solid Earth* **109**. Art No B08304, doi:10.1029/2003JB002888
- Wang, L, Wang, D, K, S (2020) Electrical conductivity of talc dehydration at high pressures and temperatures: Implications for high-conductivity anomalies in subduction zones. *J Geophys Res: Solid Earth* **125**. Art No e2020JB020091, doi:10.1029/2020JB020091
- Wei, S.S, Wiens, D.A (2018) P-wave attenuation structure of the Lau back-arc basin and implications for mantle wedge processes. *Earth Planet Sci Lett* **502**, 187–199. doi:10.1016/j.epsl.2018.09.005
- Wei, S.S, Wiens, D.A, van Keken, P.E, Cai, C (2017) Slab temperature control on the Tonga double seismic zone and slab mantle dehydration. *Sci Adv* **3**. Art No e1601755, doi:10.1126/sciadv.1601755
- Wells, R, Bukry, D, Friedman, R, Pyle, D, Duncan, R, Haeussler, P, Wooden, J (2014) Geological history of Siletzia, a large igneous province in the Oregon and Washington Coast Range: Correlation to the geomagnetic polarity time scale and implications for a long-lived Yellowstone hotspot. *Geosphere* **10**, 692–719. doi:10.1130/GES01018.1
- Wilson, C.R, Spiegelman, M.S, van Keken, P.E, Hacker, B.R (2014) Fluid flow in subduction zones: The role of solid rheology and compaction pressure. *Earth Planet Sci Lett* **401**, 261–274. doi:10.1016/j.epsl.2014.05.052
- Yin, Y, Li, C-F, Lu, Y (2021) Estimating Curie-point depths using both wavelet-based and Fourier spectral centroid methods in the western Pacific marginal seas. *Geophys J Int* **227**, 798–812. doi:10.1093/gji/ggab257
- Yoo, S, Lee, C (2023) Controls on melt focusing beneath old subduction zones: A case study of northeast Japan. *Tectonophysics* **851**. Art No 229766, doi:10.1016/j.tecto.2023.229766
- Yoshioka, S, Suminokura, Y, Matsumoto, T, Nakajima, J (2013) Two-dimensional thermal modeling of subduction of the Philippine Sea plate beneath southwest Japan. *Tectonophysics* **608**, 1094–1108.

1100 doi:10.1016/j.tecto.2013.07.003
1101 Zhao, D.P, Hasegawa, A, Kanamori, H (1994) Deep structure of the Japan subduction zone as derived from local,
1102 regional, and teleseismic events. *J Geophys Res: Solid Earth* 99, 22313–22329. doi:10.1029/94JB01149